Computational Mechanics 21 (1998) 28–47 © Springer-Verlag 1998

Synchronized reproducing kernel interpolant via multiple wavelet expansion

S. Li, W. K. Liu

Abstract In this paper, a new partition of unity – the synchronized reproducing kernel (SRK) interpolant – is derived. It is a class of meshless shape functions that exhibit synchronized convergence phenomenon: the convergence rate of the interpolation error of the higher order derivatives of the shape function can be tuned to be that of the shape function itself. This newly designed synchronized reproducing kernel interpolant is constructed as an series expansion of a scaling function kernel and the associated wavelet functions. These wavelet functions are constructed in a reproducing procedure, simultaneously with the scaling function kernel, by directly enforcing certain orders of vanishing moment conditions. To the authors knowledge, this unique interpolant is the first of its kind to be constructed, and to be used in numerical computations, both in concept and in practice. The new interpolants are in fact a group of special hierarchial meshless bases, and similar counterparts may exist in spline interpolation method, other meshless methods, Galerkin-wavelet method, as well as the finite element method.

A detailed account of the subject is presented, and the mathematical principle behind the construction procedure is further elaborated. Another important discovery of this study is that the 1st order wavelet together with the scaling function kernel can be used as a weighting function in Petrov-Galerkin procedures to provide a stable numerical computation in some pathological problems. Benchmark problems in advection-diffusion problems, and Stokes flow problem are solved by using the synchronized reproducing kernel interpolant as the weighting function. Reasonably good results have been obtained. This may open the door for designing well behaved Galerkin procedures for numerical computations in various constrained media.

Communicated by S.N. Atluri, 10 April 1997

S. Li, W.K. Liu
Department of Mechanical Engineering, Northwestern University, 2145 Sheridan Road, Evanston, IL 60208, USA

Correspondence to: W.K. Liu, e-mail: W-Liu@NWU.edu

This work is supported by grants from the Office of Naval Research, the Air Force Office of Scientific Research, and the Army Research Office. The first author (SL) is also supported by Graham-Cabell fellowship from Northwestern University.

1 Introduction

The study of meshless methods has become an area of active research in computational mechanics in the past few years. Recent surveys can be found in Belytschko et al. (1996) and Liu et al. (1996). The main focus is still placed on their abilities to circumvent the formidable task of structured or unstructured mesh generation, which is required in regular finite element methods. On the other hand, since the stringent mesh requirement is dropped, meshless methods allow more freedom in building their interpolation structures, which can lead to some nice and almost unexpected properties that are not apparent in the finite element method. This is particularly evident for reproducing kernel particle method (RKPM) because of its intrinsic structure (Liu et al. 1995; Liu et al. 1996; Liu et al. 1997). One of these interesting features is the so-called synchronized convergence phenomenon, discovered by Li and Liu (1996), which comes as a surprising result in the convergence study.

There are two types of synchronized convergence phenomena; each occurs under quite different situations. The first type of synchronized convergence phenomenon is an interior estimate, or local estimate, and it occurs for regular RKPM shape function on a uniform particle distribution with specific choices of dilation coefficients (Li and Liu 1996). By identifying the existence of such a convergence behavior, we hope to explain some phenomena observed in practice, such as the high convergence rate that occurred in numerical computations and the relief of "*locking*" for computations in constrained media. The second type of synchronized convergence phenomenon is a global estimate that is valid for all the admissible particle distributions, but the reproducing kernel used is different from the original reproducing kernel. Moreover, as far as the accuracy is concerned, the local estimate of the first type of synchronized convergence rate goes up with respect to the optimal convergence rate, because of the smoothness of the window function, whereas the global estimate of the second type of synchronized convergence rate goes down with respect to the optimal convergence rate due to the construction to meet the desired property. Nevertheless, the synchronized reproducing kernel interpolants give us many other advantages in numerical computations, which is the main focus of this paper.

A major contribution of this study is the utilization of the notion of synchronized convergence to construct multiple wavelets to form a robust partition of unity, which can be built in random particle distributions. This

type of shape functions are quite different from the regular RKPM shape function, or moving least square interpolants. The newly constructed synchronized reproducing kernel interpolant is an expansion of multiple scale reproducing kernels. Precisely speaking, the synchronized reproducing kernel interpolant designed here has two parts: a fundamental part – scaling function kernel, and a higher order part – its associated wavelet functions. It has been found that by enforcing certain vanishing moment conditions one can construct a m-term wavelet series on the original particle distribution. By combining the scaling kernel function and the wavelet functions, the so-called "synchronized reproducing kernel" is formed.

The term wavelet used in this paper follows from the rigorous mathematical definition. Nevertheless, the wavelet used to construct the synchronized reproducing kernel is a novel one, which is different from the familiar wavelets in the literature, though it may not form an orthonormal basis. In addition, the method used to generate the wavelet is also different from the popular multiresolution process, and it is also entirely different from the procedure used in Liu and Chen (1995). In recent years, wavelet analysis has achieved much success, both theoretically and pragmatically. Its applications span several areas, signal processing, image processing, digital information analysis in general; acoustic, electromagnetic wave propagation, etc. . . . . Nevertheless, the application of wavelet methods to numerical analysis, i.e. the Galerkin-wavelet method, had only a limited success. Its usefulness is limited by many factors, such as uniform discretization, rectangular domain, periodic boundary conditions, among others. The restrictions are severe that they cast an impression that the method can not deal with complex engineering computations. The approach adopted in this study is an original one, which does not follow the Galerkin wavelet method. It appears to us that the wavelets constructed in this paper may have some potential in multiple scale numerical computations.

Another remarkable discovery of this study is that if the synchronized reproducing kernel is used as a weighting function in Petrov-Galerkin procedures, it can stabilize numerical computations. Numerical experiments have been conducted to solve two types of constrained problems, advection-diffusion problem and the Stokes flow problem, by using the synchronized reproducing kernel interpolants. It is confirmed that the synchronized reproducing kernel interpolant can support almost all the current stabilized methods. This obviously furnishes a new method for designing multiple scale shape functions in standard Galerkin and Petrov-Galerkin procedures for a large class of stabilized Galerkin methods.

This paper is aimed as an independent research documentation; thus, it is arranged in a self-contained manner. In Sect. 2, the formulation of the regular reproducing kernel particle method is outlined with an emphasis on the moment expansion. In Sect. 3, the concept of synchronized convergence is introduced and elaborated. The main technical content is given in Sect. 4, where a complete procedure of constructing wavelet functions is described, and subsequently, the construction of synchronized reproducing kernel interpolants are illustrated. In Sect. 5, applications of the synchronized reproducing kernel method are discussed. Specific computation procedures, implementations, and numerical results on advection-diffusion problems, and the Stokes flow problem are documented.

2
Formulation of reproducing kernel

In this section, the formulation of the reproducing kernel method is outlined. The multiple index notation is implicitly assumed (Adams 1975). For more detail information, readers may consult Liu et al. (1995) and Liu et al. (1997).

Choosing a polynomial basis $\mathbf{P}(\mathbf{x})$, such that

$$\mathbf{P} := \{P_1, P_2, \ldots, P_\ell\}(\mathbf{x}) \tag{1}$$

with $P_1(\mathbf{x}) = 1$ and $P_i(0) = 0,\ i \neq 1$.

The m-th order reproducing kernel formula for a continuous function $u(\mathbf{x})$ in a bounded region $\Omega \subset \mathbb{R}^n$ is defined as

$$\mathscr{R}^m_\varrho u(\mathbf{x}) = \int_{\Omega_x} \mathscr{K}_\varrho(\mathbf{y}-\mathbf{x},\mathbf{x}) u(\mathbf{y})\, \mathrm{d}\Omega_\mathbf{y} \ , \tag{2}$$

$$\mathscr{R}^m_{\varrho,h} u(\mathbf{x}) = \sum_{I=1}^{np} \mathscr{K}_\varrho(\mathbf{x}_I-\mathbf{x},\mathbf{x}) u(\mathbf{x}_I) \Delta V_I \tag{3}$$

where the superscript m denotes the order of the generating polynomial basis; ϱ is the dilation parameter, which is the characteristic radius of the compact support. In most cases, $\varrho = ah$, where h is the distance between two particles, and a is the dilation coefficient. The subscript h in Eq. (3) indicates that this is a discrete interpolation form.

In Eqs.(2)–(3), the scaling function kernel and the associated correction function are defined as follows,

$$\mathscr{K}_\varrho(\mathbf{y}-\mathbf{x},\mathbf{x}) := \mathscr{C}_\varrho(\mathbf{y}-\mathbf{x},\mathbf{x}) \phi_\varrho(\mathbf{y}-\mathbf{x}) \tag{4}$$

$$\mathscr{C}_\varrho(\mathbf{y}-\mathbf{x},\mathbf{x}) := \mathbf{P}\left(\frac{\mathbf{y}-\mathbf{x}}{\varrho}\right)\mathbf{b}(\mathbf{x}) \tag{5}$$

where $\mathbf{b}(\mathbf{x})$ is an undetermined vector.

As one can see, the scaling function kernel $\mathscr{K}_\varrho$ is basically a modified window function, i.e. the product of a window function and a correction function. The correction function is defined in such a way that the following m-th order reproducing conditions are satisfied,

$$\int_\Omega P_j\left(\frac{\mathbf{y}-\mathbf{x}}{\varrho}\right)\mathscr{K}_\varrho(\mathbf{y}-\mathbf{x},\mathbf{x})\,\mathrm{d}\Omega = \delta_{j0}, \quad 1 \le j \le \ell, \tag{6}$$

Consequently, the unknown vector $\mathbf{b}(\mathbf{x})$ in Eq. (5) can be determined by the following algebraic equation

$$\mathbf{M}(\mathbf{x})\mathbf{b}(\mathbf{x}) = \mathbf{P}^t(0) \ . \tag{7}$$

More explicitly,

$$\begin{pmatrix} m_{11} & \cdots & \cdots & \cdots & m_{1n} \\ m_{21} & \ddots & & \cdots & m_{2n} \\ \vdots & & m_{ij} & & \vdots \\ \vdots & & & \ddots & \vdots \\ m_{n1} & \cdots & \cdots & \cdots & m_{nm} \end{pmatrix} \begin{pmatrix} b_1 \\ b_2 \\ \vdots \\ \vdots \\ b_n \end{pmatrix} = \begin{pmatrix} 1 \\ 0 \\ \vdots \\ \vdots \\ 0 \end{pmatrix} \ , \tag{8}$$

where the components of moment matrix are defined as[1]

$$m_{ij}(\mathbf{x}) = \int_{\Omega(\mathbf{x})} P_i(\mathbf{y}-\mathbf{x})P_j(\mathbf{y}-\mathbf{x})\phi(\mathbf{y}-\mathbf{x})\,\mathrm{d}\Omega_{\mathbf{y}} \ . \quad (9)$$

The correction function is then determined as

$$\mathscr{C}_\varrho(\mathbf{y}-\mathbf{x},\mathbf{x}) = \mathbf{P}\left(\frac{\mathbf{y}-\mathbf{x}}{\varrho}\right)\mathbf{M}^{-1}(\mathbf{x})\mathbf{P}^t(0) \ . \quad (10)$$

One may note that Eq. (8) is the basic formula of reproducing kernel method (Liu 1995; Liu et al. 1997).

30 If one chooses the polynomial basis as

$$\mathbf{P}(\mathbf{x}) = \{1, \mathbf{x}, \ldots, \mathbf{x}^\alpha, \ldots, \mathbf{x}^\gamma\}, \quad |\gamma| = m \quad (11)$$

both the continuous reproducing kernel and the discretized reproducing kernel satisfy the following m-th order reproducing conditions

$$\int_\Omega \left(\frac{\mathbf{y}-\mathbf{x}}{\varrho}\right)^\alpha \mathscr{K}_\varrho(\mathbf{y}-\mathbf{x},\mathbf{x})\,\mathrm{d}\Omega = \delta_{\alpha 0}, \quad |\alpha| \le m \quad (12)$$

$$\sum_{I=1}^{np} \left(\frac{\mathbf{x}_I-\mathbf{x}}{\varrho}\right)^\alpha \mathscr{K}_\varrho(\mathbf{x}_I-\mathbf{x},\mathbf{x})\Delta V_I = \delta_{\alpha 0}, \quad |\alpha| \le m \quad (13)$$

where α is a multiple index in $\mathbb{R}^n$, such that

$$\alpha := (\alpha_1, \alpha_2, \ldots, \alpha_n), \quad |\alpha| := \sum_{i=1}^n \alpha_i, \quad \alpha_i \ge 0 \quad (14)$$

$$\alpha! := \alpha_1!\alpha_2!\cdots\alpha_n!, \quad \mathbf{x}^\alpha := \mathbf{x}_1^{\alpha_1}\mathbf{x}_2^{\alpha_2}\cdots\mathbf{x}_n^{\alpha_n} \ ; \quad (15)$$

$$D_{\mathbf{x}}^\alpha := \partial_{\mathbf{x}_1}^{\alpha_1}\partial_{\mathbf{x}_2}^{\alpha_2}\cdots\partial_{\mathbf{x}_n}^{\alpha_n} \ . \quad (16)$$

Define the moments of the scaling function kernel as,

$$M_\alpha(\mathbf{x}) := \int_\Omega \left(\frac{\mathbf{y}-\mathbf{x}}{\varrho}\right)^\alpha \mathscr{K}_\varrho(\mathbf{y}-\mathbf{x},\mathbf{x})\,\mathrm{d}\Omega_{\mathbf{y}} \ . \quad (17)$$

The m-th order reproducing kernel conditions can be interpreted as the m-th order moment conditions,

$$M_\alpha = \delta_{0\alpha}, \qquad |\alpha| \le m \quad (18)$$

or,

$$M_0 = 1; \quad M_\alpha = 0, \quad 1 \le |\alpha| \le m \ . \quad (19)$$

Subsequently, the following m-th order completeness conditions hold[2],

$$\int_\Omega \left(\frac{\mathbf{y}-\mathbf{x}}{\varrho}\right)^\alpha D^\beta_{\mathbf{x}/\varrho}\mathscr{K}_\varrho(\mathbf{y}-\mathbf{x},\mathbf{x})\,\mathrm{d}\Omega_{\mathbf{y}} = \alpha!\delta_{\alpha\beta} \quad (20)$$

$$\sum_{I=1}^{np} \left(\frac{\mathbf{x}_I-\mathbf{x}}{\varrho}\right)^\alpha D^\beta_{\mathbf{x}/\varrho}\mathscr{K}_\varrho(\mathbf{x}_I-\mathbf{x},\mathbf{x})\Delta V_I = \alpha!\delta_{\alpha\beta} \quad (21)$$

which can also be interpreted as the following moment identity:

$$M_\alpha^{(\beta)} = \alpha!\delta_{\alpha\beta} \quad (22)$$

where

$$M_\alpha^{(\beta)}(\mathbf{x}) := \int_\Omega \left(\frac{\mathbf{y}-\mathbf{x}}{\varrho}\right)^\alpha D^\beta_{\mathbf{x}/\varrho}\mathscr{K}_\varrho(\mathbf{y}-\mathbf{x},\mathbf{x})\,\mathrm{d}\Omega_{\mathbf{y}} \ . \quad (23)$$

[1] There are two types of moments: moments of window function, m_{ij}, and moments of kernel function, M_α

[2] In this paper, we also refer them as consistency conditions

The interpolation formula (2) can be expressed as an expansion of moments,

$$\mathscr{R}_\varrho^m u(\mathbf{x}) = \sum_{|\alpha|=0}^m \partial^\alpha u(\mathbf{x}) M_\alpha(\mathbf{x})\varrho^{|\alpha|} + \varrho^{m+1}\sum_{|\alpha|=m+1}\int_\Omega \partial^\alpha u(\overline{\mathbf{x}})\left(\frac{\mathbf{y}-\mathbf{x}}{\varrho}\right)^\alpha \times \mathscr{K}_\varrho(\mathbf{y}-\mathbf{x},\mathbf{x})\,\mathrm{d}\Omega_{\mathbf{y}} \quad (24)$$

where $\overline{\mathbf{x}} := \mathbf{y} + \theta(\mathbf{x}-\mathbf{y})$, and $0 < \theta < 1$.[3]

$$\partial^\alpha u(\mathbf{x}) := \frac{1}{\alpha!}D^\alpha u(\mathbf{x}) \quad |\alpha| \le m+1 \ . \quad (25)$$

By a similar procedure, one may find that

$$D_{\mathbf{x}}^\beta\{\mathscr{R}_\varrho^m u(\mathbf{x})\} = \sum_{|\alpha|=0}^m \partial^\alpha u(\mathbf{x}) M_\alpha^{(\beta)}(\mathbf{x})\varrho^{|\alpha|-|\beta|} + \varrho^{m+1-|\beta|} \times \sum_{|\alpha|=m+1}\int_\Omega \partial^\alpha u(\overline{\mathbf{x}})\left(\frac{\mathbf{y}-\mathbf{x}}{\varrho}\right)^\alpha \times D^\beta_{\mathbf{x}/\varrho}\mathscr{K}_\varrho(\mathbf{y}-\mathbf{x},\mathbf{x})\mathrm{d}\Omega_{\mathbf{y}} \quad (26)$$

Accordingly, the truncation errors of these quantities are

$$u(\mathbf{x}) - \mathscr{R}_\varrho^m u(\mathbf{x}) = -\varrho^{m+1} \times \sum_{|\alpha|=m+1}\int_\Omega \partial^\alpha u(\overline{\mathbf{x}})\left(\frac{\mathbf{y}-\mathbf{x}}{\varrho}\right)^\alpha \mathscr{K}_\varrho(\mathbf{y}-\mathbf{x},\mathbf{x})\,\mathrm{d}\Omega_{\mathbf{y}} \ ; \quad (27)$$

$$D_{\mathbf{x}}^\beta(u(\mathbf{x}) - \mathscr{R}_\varrho^m u(\mathbf{x})) = -\varrho^{m+1-|\beta|} \times \sum_{|\alpha|=m+1}\int_\Omega \partial^\alpha u(\overline{\mathbf{x}})\left(\frac{\mathbf{y}-\mathbf{x}}{\varrho}\right)^\alpha D^\beta_{x/\varrho}\mathscr{K}_\varrho(\mathbf{y}-\mathbf{x},\mathbf{x})\,\mathrm{d}\Omega_{\mathbf{y}} \ . \quad (28)$$

Based on the consistency conditions (20) and (21), a global interpolation estimate has been established (Liu et al. 1997).

Theorem 2.1 *Assume a continuous function $u \in H^\ell(\Omega)$, and a smooth window function $\phi \in H_0^s(\Omega), s > \ell$, $s > m+1$, the interpolation error for reproducing kernel interpolants,* (2) and (3), *yield the following optimal convergence rate*

$$\|u - \mathscr{R}_\varrho^m u\|_{H^k(\Omega)} \le C_k\rho^\alpha\|u\|_{H^\ell(\Omega)} \quad (29)$$

$$\|u - \mathscr{R}_{\varrho,h}^m u\|_{H^k(\Omega)} \le C'_k\rho^\alpha\|u\|_{H^\ell(\Omega)} \quad (30)$$

where

$$\alpha = \min\{\ell-k, \ell+1-k\}, \quad \textit{with } 0 \le k \le m \ . \quad (31)$$

3
Synchronized convergence

One of the technical ingredients of the reproducing kernel method is to embed a very smooth window function into

[3] If the sub-domain $\mathrm{supp}\{\phi(\mathbf{y}-\mathbf{x})\} \cap \Omega$ is star-shaped, it is always true that $\overline{\mathbf{x}} \in \Omega$.

the scaling function kernel. Thus, in order to achieve the same optimal convergence rate, an extra computation effort is needed in comparison with the finite element method. This is true because the optimal convergence rate of RKPM is controlled by the order of generating polynomial basis, regardless of the smoothness of the window function. A natural question is: can we exploit the situation? The answer is yes. After careful study, we find that if one can enforce the correction function to be constant in a local region, and the embedded window function satisfies certain smoothness condition, such as the higher order Strang-Fix condition (Strang and Fix 1973; de Boor and Jia 1985), one can expect a synchronized convergence phenomenon, that is, within a certain range, the convergence rates of all the relevant H-norm will increase from their optimal rate to the convergence rate of L_2 error norm. Although this is a significant improvement, it only happens under severe restrictions such as uniform particle distributions, and integer dilation coefficients. Subsequently the method loses its meshless flavor. Moreover, the synchronized convergence estimate obtained in Li and Liu (1996) is only a local estimate, which may or may not have background effect on quasi-uniform particle distribution, though it is believed that this is one of the reasons why moving least square based meshless methods can relieve "*locking*" for computations in constrained media.

Nevertheless, to understand the mathematical principle behind the synchronized convergence may be more important than the numerical phenomenon itself. By doing so, the convergence mechanism can be controlled and utilized towards our advantages in numerical computations.

3.1
An heuristic example

We start with a simple, one-dimensional example to illustrate the basic notion of synchronized convergence. Assume that the generating polynomial order is one, i.e. $m = 1$.

$$\mathbf{P}(\mathbf{x}) = (1, x) \ , \tag{32}$$

and the embedded window function $\phi \in H^s(\mathbb{R}), s > 2$. For a continuous function $u \in H^2(\Omega)$, the continuous reproducing kernel formula reads as

$$\mathscr{R}^m_\varrho u(x) = \int_\Omega \mathscr{K}_\varrho(y - x, x) u(y)\, \mathrm{d}\Omega \ . \tag{33}$$

By Taylor's expansion, we arrive at a particular form of Eq. (24),

$$\begin{aligned}\mathscr{R}^m_\varrho u(x) &= \int_\Omega \mathscr{K}_\varrho(y - x, x)\{u(x) + u_{,x}(x)(y - x) \\ &\quad + \frac{1}{2!} u_{,xx}(x)(y - x)^2 + \cdots\}\mathrm{d}y \\ &= u(x)M_0(x) + \varrho u^{(1)}(x)M_1(x) \\ &\quad + \frac{\varrho^2}{2!} u^{(2)}(x)M_2(x) + \frac{\varrho^3}{3!} u^{(3)}(x)M_3(x) \\ &\quad + \frac{\varrho^4}{4!} u^{(4)}(x)M_4(x) + \mathscr{O}(\varrho^5)\end{aligned} \tag{34}$$

where

$$u^{(n)} := D^n_x u(x) \tag{35}$$

Proceeding similarly, one may derive

$$\begin{aligned}D_x\{\mathscr{R}^m_\varrho u(x)\} &= \int_\Omega D_x \mathscr{K}_\varrho(y - x, x) u(y)\mathrm{d}\Omega \\ &= \frac{1}{\varrho} u(x)M^{(1)}_0(x) + u^{(1)}(x)M^{(1)}_1(x) \\ &\quad + \frac{\varrho}{2!} u^{(2)}(x)M^{(1)}_2(x) \\ &\quad + \frac{\varrho^2}{3!} u^{(3)}(x)M^{(1)}_3(x) + \frac{\varrho^3}{4!} u^{(4)}(x) \\ &\quad \times M^{(1)}_4(x) + \mathscr{O}(\varrho^4)\end{aligned} \tag{36}$$

where

$$M^{(j)}_i(x) := \int_\Omega \left(\frac{y - x}{\varrho}\right)^i D^j_{x/\varrho} \mathscr{K}_\varrho(y - x, x)\mathrm{d}\Omega_{\mathrm{y}} \tag{37}$$

and

$$\begin{aligned}D^2_x\{\mathscr{R}^m_\varrho u(x)\} &= \int_\Omega D^2_x \mathscr{K}_\varrho(y - x, x) u(y)\mathrm{d}\Omega \\ &= \frac{1}{\varrho^2} u(x)M^{(2)}_0(x) + \frac{1}{\varrho} u^{(1)}(x)M^{(2)}_1(x) \\ &\quad + \frac{1}{2!} u^{(2)}(x)M^{(2)}_2(x) + \frac{\varrho}{3!} u^{(3)}(x)M^{(2)}_3(x) \\ &\quad + \frac{\varrho^2}{4!} u^{(4)}(x)M^{(2)}_4(x) \\ &\quad + \mathscr{O}(\varrho^3) \ .\end{aligned} \tag{38}$$

In Table 1, the three quantities, $(u - \mathscr{R}^m_\varrho u)$, $D_x(u - \mathscr{R}^m_\varrho u)$, and $D^2_x(u - \mathscr{R}^m_\varrho u)$, are tabulated in the order of dilation parameter ϱ. By reproducing conditions, the following moment conditions hold,

Table 1. Pointwise truncation errors

Completeness conditions			Truncation errors		
$u - \mathscr{R}^m_\varrho u =$	$u(1 - M_0)$	$-\varrho u^{(1)} M_1$	$-\frac{\varrho^2}{2!} u^{(2)} M_2$	$-\frac{\varrho^3}{3!} u^{(3)} M_3$	$-\frac{\varrho^4}{4!} u^{(4)} M_4$
			$\mathscr{O}(\varrho^2)$	$\mathscr{O}(\varrho^3)$	$\mathscr{O}(\varrho^4)$
$D_x(u - \mathscr{R}^m_\varrho u) =$	$-\frac{1}{\varrho} u M^{(1)}_0$	$u^{(1)}(1 - M^{(1)}_1)$	$-\frac{\varrho}{2!} u^{(2)} M^{(1)}_2$	$-\frac{\varrho^2}{3!} u^{(3)} M^{(1)}_3$	$-\frac{\varrho^3}{4!} u^{(4)} M^{(1)}_4$
			$\mathscr{O}(\varrho)$	$\mathscr{O}(\varrho^2)$	$\mathscr{O}(\varrho^3)$
$D^2_x(u - \mathscr{R}^m_\varrho u) =$	$-\frac{1}{\varrho^2} u M^{(2)}_0$	$-\frac{1}{\varrho} u^{(1)} M^{(2)}_1$	$u^{(2)}(1 - \frac{1}{2!} M^{(2)}_2)$	$-\frac{\varrho}{3!} u^{(3)} M^{(2)}_3$	$-\frac{\varrho^2}{4!} u^{(4)} M^{(2)}_4$
			$\mathscr{O}(\varrho^0)$	$\mathscr{O}(\varrho)$	$\mathscr{O}(\varrho^2)$

$$M_0 = 1, \quad M_1 = 0 \ , \tag{39}$$

from which, one can further deduce that

$$M_0^{(1)} = 0, \quad M_0^{(2)} = 0 \ ; \tag{40}$$

$$M_1^{(1)} = 1, \quad M_1^{(2)} = 0 \ . \tag{41}$$

From Table 1, it is quite clear that the conditions (39)–(41) enforce the truncation errors for quantities $(u - \mathscr{R}_\varrho^m u)$, $D_x(u - \mathscr{R}_\varrho^m u)$, and $D_x^2(u - \mathscr{R}_\varrho^m u)$ to be in the order of $\mathscr{O}(\varrho^2)$, $\mathscr{O}(\varrho)$ and $\mathscr{O}(1)$, respectively. This also implies that the global interpolation error for L_2, H_1 and H_2 norms are in the order of $\mathscr{O}(\varrho^2)$, $\mathscr{O}(\varrho)$, and $\mathscr{O}(1)$, correspondingly, which are the usual optimal convergence rates, as indicated in Theorem 2.1.

3.2 Synchronized convergence

If there is any possibility that synchronized convergence could happen, i.e. the L_2, H_1, and H_2 error norm have the same convergence rate, the local truncation errors of $(u - \mathscr{R}_\varrho^m u)$, $D_x(u - \mathscr{R}_\varrho^m u)$, and $D_x^2(u - \mathscr{R}_\varrho^m u)$ have to be at the same order, as the pattern indicated in Table 1. In other words, all the quantities below the shaded "ladder" in Table 1 should be zero. This requires additional moment conditions as indicated in Table 2. That is

$$M_2^{(1)} = 0 \tag{42}$$

$$M_2^{(2)} = 2!, \quad M_3^{(2)} = 0 \ . \tag{43}$$

One can verify that these additional moment conditions (42)–(43) are satisfied, if moments M_2, M_3 are constants. In general, they are not constant, because for the case $m = 1$ only two moment conditions are enforced, i.e. Eq. (39). Exception arise, if one can enforce the correction function to be constant. In that case, in the interior domain, M_2, M_3, and even higher order moments take constant values. But, there is another difficulty, i.e. in actual computations, generally speaking, the discrete moments M_2^h, M_3^h are always functions of x, because

$$M_2^h(x) = \sum_{I=1}^{np} \left(\frac{x_I - x}{\varrho}\right)^2 \mathscr{K}_\varrho(x_I - x, x)\Delta x_I \ , \tag{44}$$

$$M_3^h(x) = \sum_{I=1}^{np} \left(\frac{x_I - x}{\varrho}\right)^3 \mathscr{K}_\varrho(x_I - x, x)\Delta x_I \ , \tag{45}$$

even if $M_2 = \text{constant}$, $M_3 = \text{constant}$. However, the difficulty can be circumvented if the embedded window function has nice properties, such as it satisfies the higher order Strang-Fix conditions (Strang and Fix 1973; Li and Liu 1996). In that case, indeed, the higher order discrete moments can be constant on uniform particle distribution, i.e.

Table 2. Moment conditions

Moment conditions		Additional conditions	
$M_0 = 1$	$M_1 = 0$		
$M_0^{(1)} = 0$	$M_1^{(1)} = 1!$	$M_2^{(1)} = 0$	
$M_0^{(2)} = 0$	$M_1^{(2)} = 0$	$M_2^{(2)} = 2!$	$M_3^{(2)} = 0$

$$M_2^h = M_2 = \text{constant}, \quad M_3^h = M_3 = \text{constant} \tag{46}$$

Consequently, the additional moment conditions in Table 2 are automatically satisfied, as proved in Li and Liu (1996). Under these particular circumstances, the reproducing kernel interpolants can achieve the so-called synchronized convergence. For detail information, readers can consult Li and Liu (1996). The main result is listed as follows.

Define the Fourier transform of the window function ϕ as,

$$\hat{\phi}(\zeta) := \int_{\mathbb{R}^n} \phi(z) \exp(-i\zeta z) \mathrm{d}z \tag{47}$$

and the set of functions that satisfy the p-th order Strang-Fix condition as,

$$SF_h^{(p)} := \{\phi | \hat{\phi}(0) = 1, D_\zeta^\alpha \hat{\phi}\left(\frac{2\pi j}{h}\right) 0, \quad \forall j \in \mathbf{Z}^n \backslash \{0\}, \quad |\alpha| \le p\} \ . \tag{48}$$

Theorem 3.1 *Assume that* $u \in H^{m+s+1}(\Omega)$, $\phi \in SF_{1/a}^{(m+s+1)}$ *where* $a = \varrho/h$, *and the correction function* $\mathscr{C}_\varrho^h(y - x, x) = \text{const.}\ \forall x \in \Omega_0 \subset \text{int}(\Omega)$. *Then, the m-th order RKPM interpolants can achieve a synchronized convergence rate in* Ω_0, *i.e.*

$$\|u - \mathscr{R}_{\varrho,h}^m u\|_{H^k(\Omega_0)} \le C_k \varrho^{m+1} \|u\|_{H^{m+k+1}(\Omega_0)}, \quad 0 \le k \le s \ . \tag{49}$$

Remark 3.1. *The synchronized convergence result stated in Theorem* (3.1) *is a striking improvement in comparison with the usual optimal convergence rate. The primary reason responsible for synchronized convergence is the smoothness of the window function, which is not being utilized if the particle distribution is random, or irregular. However, if the particles can be arranged into a uniform distribution in a local region, one may take advantage of the smoothness of the window function embedded, and observe the leap in the convergence rates.*

Example 3.1 *Numerical tests have been performed to verify the theorem. We used both the cubic spline* $(\phi \in SF^{(4)})$ *and the fifth order spline* $(\phi \in SF^{(6)})$ *as window function with a polynomial basis* $(1, x)$ *in a uniform particle distribution* $(\varrho = 1 \cdot h)$ *to form the reproducing kernel partition unity in 1-D line segment* [0, 1]. *Then, these shape functions are employed to solve the following ODE in a standard Galerkin procedure,*

$$-\frac{\mathrm{d}^2}{\mathrm{d}x^2} u + u = f(x), \quad x \in (0, 1) \tag{50}$$

$$\left.\frac{\mathrm{d}u}{\mathrm{d}x}\right|_{x=-1} = -6, \quad \left.\frac{\mathrm{d}u}{\mathrm{d}x}\right|_{x=1} = 6; \quad f(x) = x^6 - 30.0x^4 \ ; \tag{51}$$

The convergence rates are measured from different set of computations, in which the number of particles varies from 21 *to* 201. *Taking out a segment* 5% *of total length at each end, we plot the error of numerical solutions in Fig.* 1. *One can observe the synchronized convergence phenomenon.*

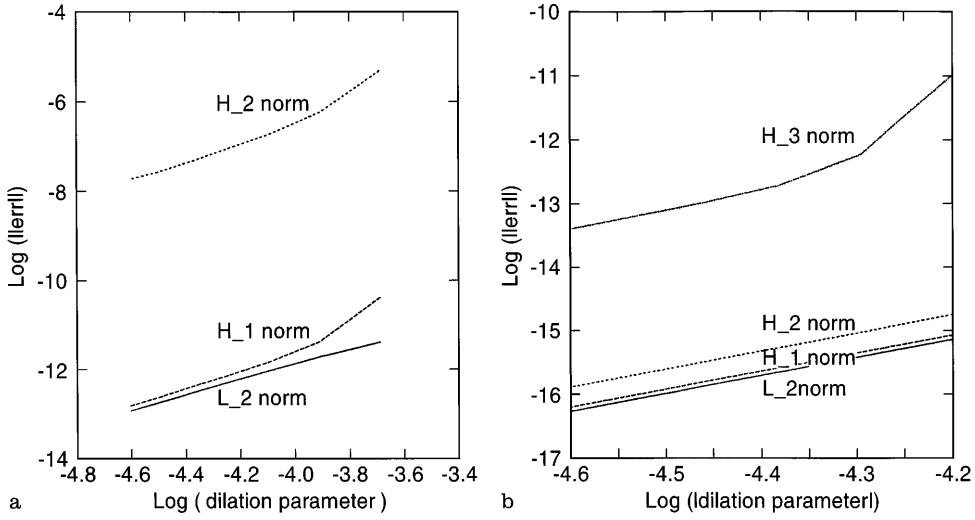

Fig. 1a, b. The synchronized convergence: **a** The cubic spline; **b** The fifth order spline

However, one should be reminded that the results plotted in Fig. 1 *are not the actual interpolation error; they are the errors of numerical solutions.*

4
Synchronized reproducing interpolants via multiple wavelet expansion

The synchronized convergence Theorem 3.1 is a local estimate in nature, because, for most practical problems, the correction function near the boundary is not constant. Moreover, Theorem 3.1 is only valid for uniform particle distribution as required in the theorem, which suggests that, in order to achieve the desirable convergence rate, we have to sacrifice the prime virtue of meshless method.

On the other hand, we have learned that synchronized convergence can be achieved by maneuvering moment conditions to control the truncation errors. Thus, based on the same convergence mechanism, one may design a particular kernel function, whose truncation errors have a "ladder" structure, as illustrated in Table 1. Consequently, this kernel interpolant will genetically possess the synchronized convergence property. Followed this idea, we propose a constructive approach to design a new type of reproducing kernel – synchronized reproducing kernel, which has synchronized convergence property inherently, and is also valid for any admissible particle distributions.

4.1
Multiple wavelet expansion

The so-called synchronized reproducing kernel interpolants are constructed through a multiple scale expansion process. Let $\mathscr{K}_{\varrho}^{[s]}$ denote a synchronized reproducing kernel interpolant. For a basis of m-th order generating polynomial, we define the synchronized reproducing kernel as

$$\mathscr{K}_{\varrho}^{[s]}(\cdot,\cdot) := \sum_{|\beta|=0}^{m} C_{\beta}\mathscr{K}_{\varrho}^{[\beta]}(\cdot,\cdot) \ , \tag{52}$$

where β is a multiple index. Hereafter the Greek letter, or number in the square bracket of a superscript indicates the order of the kernel function as defined in (52); meanwhile the letter in parenthesis in the superscript remains to denote partial derivatives as defined in either (35) or (37). In Eq. (52), $\mathscr{K}_{\varrho}^{[s]}$ and $\mathscr{K}_{\varrho}^{[0]}$ are referred to as the synchronized reproducing kernel and the scaling function kernel respectively. The scaling function kernel is the regular reproducing kernel defined in (2), which carries the information of the fundamental scale. For the rest of the series, $\mathscr{K}_{\varrho}^{[\beta]}, \beta \neq 0$, are called the wavelet functions, which carry information of higher order scales.

To keep a consistent notation, we distinguish the moments from different kernels i.e.

$$M_{\alpha}^{[\beta]}(\mathbf{x}) := \int_{\Omega}\left(\frac{\mathbf{y}-\mathbf{x}}{\varrho}\right)^{\alpha}\mathscr{K}_{\varrho}^{[\beta]}(\mathbf{y}-\mathbf{x},\mathbf{x})\mathrm{d}\Omega_{\mathbf{y}} \ . \tag{53}$$

Then the consistent conditions for every kernel function, $\mathscr{K}_{\varrho}^{[\beta]}$, can be described in an unified manner

$$M_{\beta}^{[\beta]} = 1 \ , \tag{54}$$

$$M_{\alpha}^{[\beta]} = 0, \quad \alpha \neq \beta, \quad |\alpha| \leq m \ . \tag{55}$$

Equivalently,

$$\int_{\Omega}\left(\frac{\mathbf{y}-\mathbf{x}}{\varrho}\right)^{\beta}\mathscr{K}_{\varrho}^{[\beta]}(\mathbf{y}-\mathbf{x},\mathbf{x})\mathrm{d}\Omega_{\mathbf{y}} = 1 \ , \tag{56}$$

$$\int_{\Omega}\left(\frac{\mathbf{y}-\mathbf{x}}{\varrho}\right)^{\alpha}\mathscr{K}_{\varrho}^{[\beta]}(\mathbf{y}-\mathbf{x},\mathbf{x})\mathrm{d}\Omega_{\mathbf{y}} = 0,$$
$$\beta \neq \alpha, \quad |\alpha| \leq m \ . \tag{57}$$

There is no summation on β in (54) and (56).

It is obvious that if $|\beta| \neq 0$ then kernel $\mathscr{K}_{\varrho}^{[\beta]}$ satisfies $|\beta| - 1$ order vanishing moment conditions, i.e.

$$\int_{\Omega}\left(\frac{\mathbf{y}-\mathbf{x}}{\varrho}\right)^{\alpha}\mathscr{K}_{\varrho}^{[\beta]}(\mathbf{y}-\mathbf{x},\mathbf{x})\mathrm{d}\Omega_{\mathbf{y}} = 0, \quad 0 \leq |\alpha| \leq |\beta| - 1 \tag{58}$$

In other words, it is always true that [4]

In the infinite domain, such as $\mathbb{R}^n$, or interior domain $\mathrm{dist}(\mathbf{x}, \partial\Omega) > 0, \mathscr{K}_{\varrho}^{[\beta]}(\mathbf{z},\mathbf{x}) = \mathscr{K}_{\varrho}^{[\beta]}(\mathbf{z})$

$$\int_{\mathbb{R}^n} \mathscr{K}_{\varrho}^{[\beta]}(\mathbf{z})\mathrm{d}\Omega_z = 0, \qquad \forall|\beta| \neq 0 \tag{59}$$

In our construction, we always assume that the window function $\phi \in L_2(\mathbb{R})$, and it is also compact supported; thus, $\mathscr{K}_{\varrho}^{[\beta]} \in L_1(\mathbb{R}^n) \cap L_2(\mathbb{R}^n)$. Therefore,

$$|\hat{\mathscr{K}}_{\varrho}^{[\beta]}(\zeta)| = |\hat{\mathscr{K}}_{\varrho}^{[\beta]}(-\zeta)| \ , \tag{60}$$

which immediately leads to (see Chui 1992; Daubechies 1992 for details)

$$C_\psi/2 = \pi \int_0^\infty \frac{\mathrm{d}\zeta}{\zeta} |\hat{\mathscr{K}}_{\varrho}^{[\beta]}(\zeta)|^2 < +\infty \ . \tag{61}$$

This is precisely the admissible condition of wavelet (Kaiser 1994). As a matter of fact, based on the definition of Grossmann and Morlet (Meyer 1993; Chui 1992), a wavelet is a function ψ in $L_2(\mathbb{R})$ whose Fourier transform $\hat{\psi}(\zeta)$ satisfies the condition

$$\int_0^\infty |\hat{\psi}(\zeta)|^2 \frac{\mathrm{d}\zeta}{\zeta} = 1 \ . \tag{62}$$

Hence, the higher order kernels $\mathscr{K}_{\varrho}^{[\beta]}, |\beta| \neq 0$, in our formulation differ at most a coefficient factor with the usual wavelet (meaning the orthonormal wavelet!). Thus, indeed, they are legitimate wavelets, though in most of cases, they may not form an orthonormal basis. This is the reason why we call $\mathscr{K}_{\varrho}^{[\beta]}$ as wavelet function, when $|\beta| \neq 0$. A detailed analysis of the mathematical aspect of this particular class of wavelets is prepared in a forthcoming paper (Li and Liu 1997).

To demonstrate the construction procedures, we proceed with the construction of several commonly used kernel functions.

Example 4.1 *Assume $m = 1$ and $\mathbf{P} = (1, x)$. The associated synchronized reproducing kernel interpolant can be expressed as*

$$\mathscr{K}_{\varrho}^{[s]}(\cdot,\cdot) = \mathscr{K}_{\varrho}^{[0]}(\cdot,\cdot) + \mathscr{K}_{\varrho}^{[1]}(\cdot,\cdot) \tag{63}$$

in which, the scaling function kernel satisfies the fundamental moment conditions,

$$M_0^{[0]} = 1, \quad M_1^{[0]} = 0 \ . \tag{64}$$

Since,

$$\mathscr{K}_{\varrho}^{[0]}(y-x,x) = \mathbf{P}\left(\frac{y-x}{\varrho}\right)\mathbf{b}^{(0)}(x)\phi_\varrho(y-x) \ , \tag{65}$$

Eq. (64) is equivalent to

$$\begin{pmatrix} m_0 & m_1 \\ m_1 & m_2 \end{pmatrix}\begin{pmatrix} b_1^{(0)} \\ b_2^{(0)} \end{pmatrix} = \begin{pmatrix} 1 \\ 0 \end{pmatrix} \tag{66}$$

On the other hand, the first "wavelet" function has to satisfy the following moment conditions,

$$M_0^{[1]} = 0; \qquad M_1^{[1]} = 1 \ . \tag{67}$$

Assume

$$\mathscr{K}_{\varrho}^{[1]}(y-x,x) = \mathbf{P}\left(\frac{y-x}{\varrho}\right)\mathbf{b}^{(1)}(x)\phi_\varrho(y-x) \ , \tag{68}$$

The unknown vector $\mathbf{b}^{(1)}$ is determined by

$$\begin{pmatrix} m_0 & m_1 \\ m_1 & m_2 \end{pmatrix}\begin{pmatrix} b_1^{(1)} \\ b_2^{(1)} \end{pmatrix} = \begin{pmatrix} 0 \\ 1 \end{pmatrix} \tag{69}$$

The scaling function kernel and wavelet constructed in Example (4.1) is plotted in Fig. 2. The cubic spline is used as the window function; the dilation parameter is chosen as $\varrho = 1 \cdot h$.

Example 4.2 *Let $m = 2$ and $\mathbf{P} = (1, x, x^2)$. The associated synchronized reproducing kernel can be expressed as*

$$\mathscr{K}_{\varrho}^{[s]}(\cdot,\cdot) = \sum_{\beta=0}^{2} C_\beta \mathscr{K}_{\varrho}^{[\beta]}(\cdot,\cdot) \tag{70}$$

where

$$\mathscr{K}_{\varrho}^{[\beta]}(y-x,x) = \mathbf{P}\left(\frac{y-x}{\varrho}\right)\mathbf{b}^{(\beta)}(x)\phi_\varrho(y-x), \quad 0 \leq \beta \leq 2 \tag{71}$$

In (71), $\mathbf{b}^{(0)}$, $\mathbf{b}^{(1)}$, *and* $\mathbf{b}^{(2)}$ *satisfy the following algebraic equations respectively,*

$$\begin{pmatrix} m_0 & m_1 & m_2 \\ m_1 & m_2 & m_3 \\ m_2 & m_3 & m_4 \end{pmatrix}\begin{pmatrix} b_1^{(0)} \\ b_2^{(0)} \\ b_3^{(0)} \end{pmatrix} = \begin{pmatrix} 1 \\ 0 \\ 0 \end{pmatrix} \tag{72}$$

$$\begin{pmatrix} m_0 & m_1 & m_2 \\ m_1 & m_2 & m_3 \\ m_2 & m_3 & m_4 \end{pmatrix}\begin{pmatrix} b_1^{(1)} \\ b_2^{(1)} \\ b_3^{(1)} \end{pmatrix} = \begin{pmatrix} 0 \\ 1 \\ 0 \end{pmatrix} \tag{73}$$

$$\begin{pmatrix} m_0 & m_1 & m_2 \\ m_1 & m_2 & m_3 \\ m_2 & m_3 & m_4 \end{pmatrix}\begin{pmatrix} b_1^{(2)} \\ b_2^{(2)} \\ b_3^{(2)} \end{pmatrix} = \begin{pmatrix} 0 \\ 0 \\ 1 \end{pmatrix} \tag{74}$$

The scaling kernel function and its associated wavelets in Example (4.2) are plotted in Fig. 3. In Fig. 3, the fifth order spline is used as the window function, and the dilation parameter $\varrho = 1.1 \cdot h$. One may notice that in Fig. 3b the 2nd wavelet resembles an upside down Mexican hat; it is, however, compact supported unlike the formal Mexican hat wavelet (Daubechies 1992).

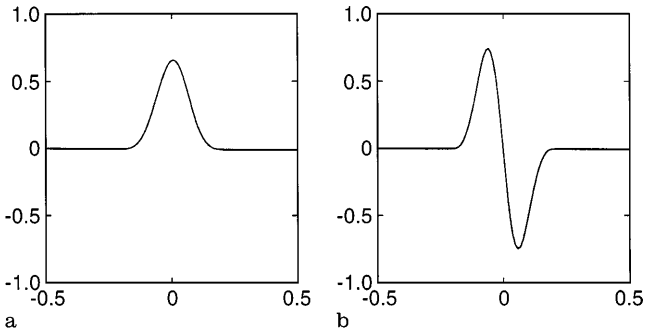

Fig. 2a, b. Scaling kernel and wavelet for basis $(1, x)$: **a** Scaling function kernel: **b** Wavelet function

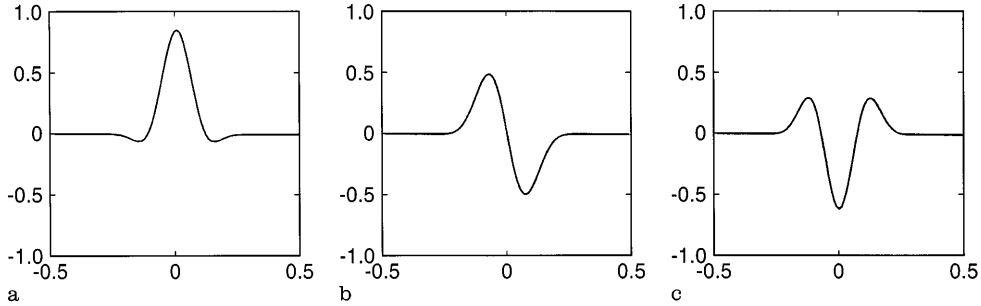

Fig. 3a–c. Scaling function kernel and wavelets for basis $(1, x, x^2)$: **a** Scaling function kernel; **b** The 1st wavelet; **c** The 2nd wavelet

Example 4.3 *Let $m = 3$ and $\mathbf{P} = (1, x, x^2, x^3)$. The associated synchronized reproducing kernel is*

$$\mathscr{K}_{\varrho}^{[s]}(\cdot,\cdot) = \sum_{\beta=0}^{3} C_\beta \mathscr{K}_{\varrho}^{[\beta]}(\cdot,\cdot) \tag{75}$$

where

$$\mathscr{K}_{\varrho}^{[\beta]}(y-x,x) = \mathbf{P}^t\left(\frac{y-x}{\varrho}\right)\mathbf{b}^{(\beta)}(x)\phi_\varrho(y-x) \tag{76}$$

in which the unknown vectors, $\mathbf{b}^{(\beta)}$, are determined by the moment conditions,

$$M_\beta^{[\beta]} = 1, \quad M_\alpha^{[\beta]} = 0, \quad \alpha \neq \beta, \quad |\alpha| \leq m \ . \tag{77}$$

That is

$$\begin{pmatrix} m_0 & m_1 & m_2 & m_3 \\ m_1 & m_2 & m_3 & m_4 \\ m_2 & m_3 & m_4 & m_5 \\ m_3 & m_4 & m_5 & m_6 \end{pmatrix} \begin{pmatrix} b_1^{(0)} \\ b_2^{(0)} \\ b_3^{(0)} \\ b_4^{(0)} \end{pmatrix} = \begin{pmatrix} 1 \\ 0 \\ 0 \\ 0 \end{pmatrix} \tag{78}$$

$$\begin{pmatrix} m_0 & m_1 & m_2 & m_3 \\ m_1 & m_2 & m_3 & m_4 \\ m_2 & m_3 & m_4 & m_5 \\ m_3 & m_4 & m_5 & m_6 \end{pmatrix} \begin{pmatrix} b_1^{(1)} \\ b_2^{(1)} \\ b_3^{(1)} \\ b_4^{(1)} \end{pmatrix} = \begin{pmatrix} 0 \\ 1 \\ 0 \\ 0 \end{pmatrix} \tag{79}$$

$$\begin{pmatrix} m_0 & m_1 & m_2 & m_3 \\ m_1 & m_2 & m_3 & m_4 \\ m_2 & m_3 & m_4 & m_5 \\ m_3 & m_4 & m_5 & m_6 \end{pmatrix} \begin{pmatrix} b_1^{(2)} \\ b_2^{(2)} \\ b_3^{(2)} \\ b_4^{(2)} \end{pmatrix} = \begin{pmatrix} 0 \\ 0 \\ 1 \\ 0 \end{pmatrix} \tag{80}$$

$$\begin{pmatrix} m_0 & m_1 & m_2 & m_3 \\ m_1 & m_2 & m_3 & m_4 \\ m_2 & m_3 & m_4 & m_5 \\ m_3 & m_4 & m_5 & m_6 \end{pmatrix} \begin{pmatrix} b_1^{(3)} \\ b_2^{(3)} \\ b_3^{(3)} \\ b_4^{(3)} \end{pmatrix} = \begin{pmatrix} 0 \\ 0 \\ 0 \\ 1 \end{pmatrix} \tag{81}$$

The scaling function kernel and its associated wavelets in Example (4.3) are displayed in Fig. 4. In the actual construction, the fifth order spline is used as the window function, and the dilation parameter is chosen as $\varrho = 1.1 \cdot h$.

Example 4.4 *This is a 2-D example. Assume $m = 1$ and $\mathbf{P} = (1, x_1, x_2)$. The associated synchronized reproducing kernel is*

$$\mathscr{K}_{\varrho}^{[s]}(\cdot,\cdot) = \sum_{|\beta|=0}^{1} C_\beta \mathscr{K}_{\varrho}^{[\beta]}(\cdot,\cdot) \tag{82}$$

where

$$\mathscr{K}_{\varrho}^{[\beta]}(\mathbf{y}-\mathbf{x},\mathbf{x}) = \mathbf{P}^t\left(\frac{\mathbf{y}-\mathbf{x}}{\varrho}\right)\mathbf{b}^{(\beta)}(\mathbf{x})\phi_\varrho(\mathbf{y}-\mathbf{x}),$$
$$0 \leq |\beta| \leq 1 \tag{83}$$

and β is multiple index, i.e. $\beta = (\beta_1, \beta_2)$, and

$$|\beta| = \beta_1 + \beta_2 \ . \tag{84}$$

The unknown vectors, $\mathbf{b}^{(0,0)}$, $\mathbf{b}^{(1,0)}$, and $\mathbf{b}^{(0,1)}$, have to satisfy the following synchronized reproducing moment conditions,

$$M_\beta^{[\beta]} = 1, \quad M_\alpha^{[\beta]} = 0, \quad \alpha \neq \beta, \quad 0 \leq |\alpha| \leq 1 \ . \tag{85}$$

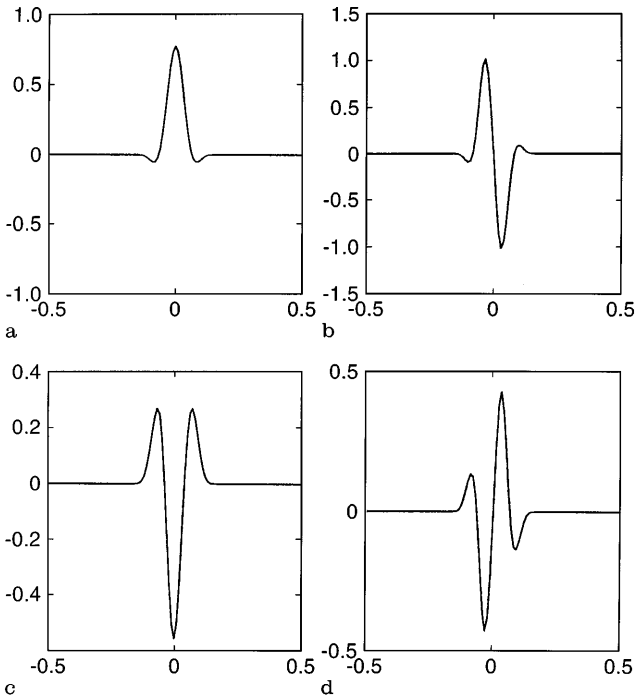

Fig. 4a–d. Scaling function kernel and wavelets for basis $(1, x, x^2, x^3)$: **a** Scaling function kernel; **b** The 1st wavelet; **c** The 2nd wavelet; **d** The 3rd wavelet

Define

$$m_{ij}(\mathbf{x}) := \int_{\Omega} y_1^i y_2^j \phi(\mathbf{y}-\mathbf{x})\mathrm{d}\Omega \ . \tag{86}$$

The moment conditions (85) can be explicitly expressed as follows

$$\begin{pmatrix} m_{00} & m_{10} & m_{01} \\ m_{10} & m_{20} & m_{11} \\ m_{01} & m_{11} & m_{02} \end{pmatrix} \begin{pmatrix} b_1^{(0,0)} \\ b_2^{(0,0)} \\ b_3^{(0,0)} \end{pmatrix} = \begin{pmatrix} 1 \\ 0 \\ 0 \end{pmatrix} \tag{87}$$

$$\begin{pmatrix} m_{00} & m_{10} & m_{01} \\ m_{10} & m_{20} & m_{11} \\ m_{01} & m_{11} & m_{02} \end{pmatrix} \begin{pmatrix} b_1^{(1,0)} \\ b_2^{(1,0)} \\ b_3^{(1,0)} \end{pmatrix} = \begin{pmatrix} 0 \\ 1 \\ 0 \end{pmatrix} \tag{88}$$

$$\begin{pmatrix} m_{00} & m_{10} & m_{01} \\ m_{10} & m_{20} & m_{11} \\ m_{01} & m_{11} & m_{02} \end{pmatrix} \begin{pmatrix} b_1^{(0,1)} \\ b_2^{(0,1)} \\ b_3^{(0,1)} \end{pmatrix} = \begin{pmatrix} 0 \\ 0 \\ 1 \end{pmatrix} \tag{89}$$

The resulting scaling function kernel and wavelets are shown in Fig. 5. In this case, the 2-D cubic spline is used as the window function, and the dilation vector is $\varrho_1 = 1 \cdot h_{x1},\ \varrho_2 = 1 \cdot h_{x2}$.

Example 4.5 *In this example, an incomplete second order polynomial basis is used. It can produce a partition of unity for the particle distribution on a 2-D square domain, which satisfies essential boundary condition. Let* $\mathbf{P} = (1, x_1, x_2, x_1 x_2)$, *and*

$$\mathscr{K}_{\varrho}^{[s]}(\cdot,\cdot) = \sum_{|\beta|=0}^{2} C_\beta \mathscr{K}_{\varrho}^{[\beta]}(\cdot,\cdot) \tag{90}$$

$$\mathscr{K}_{\varrho}^{[\beta]}(\mathbf{y}-\mathbf{x},\mathbf{x}) = \mathbf{P}\left(\frac{\mathbf{y}-\mathbf{x}}{\varrho}\right)\mathbf{b}^{(\beta)}(\mathbf{x}) \tag{91}$$

where the unknown vectors $\mathbf{b}^{(\beta)}$ *satisfy the following moment equations,*

$$\begin{pmatrix} m_{00} & m_{10} & m_{01} & m_{11} \\ m_{10} & m_{20} & m_{11} & m_{21} \\ m_{01} & m_{11} & m_{02} & m_{12} \\ m_{11} & m_{21} & m_{12} & m_{22} \end{pmatrix} \begin{pmatrix} b_1^{(0,0)} \\ b_2^{(0,0)} \\ b_3^{(0,0)} \\ b_4^{(0,0)} \end{pmatrix} = \begin{pmatrix} 1 \\ 0 \\ 0 \\ 0 \end{pmatrix} \tag{92}$$

$$\begin{pmatrix} m_{00} & m_{10} & m_{01} & m_{11} \\ m_{10} & m_{20} & m_{11} & m_{21} \\ m_{01} & m_{11} & m_{02} & m_{12} \\ m_{11} & m_{21} & m_{12} & m_{22} \end{pmatrix} \begin{pmatrix} b_1^{(1,0)} \\ b_2^{(1,0)} \\ b_3^{(1,0)} \\ b_4^{(1,0)} \end{pmatrix} = \begin{pmatrix} 0 \\ 1 \\ 0 \\ 0 \end{pmatrix} \tag{93}$$

$$\begin{pmatrix} m_{00} & m_{10} & m_{01} & m_{11} \\ m_{10} & m_{20} & m_{11} & m_{21} \\ m_{01} & m_{11} & m_{02} & m_{12} \\ m_{11} & m_{21} & m_{12} & m_{22} \end{pmatrix} \begin{pmatrix} b_1^{(0,1)} \\ b_2^{(0,1)} \\ b_3^{(0,1)} \\ b_4^{(0,1)} \end{pmatrix} = \begin{pmatrix} 0 \\ 0 \\ 1 \\ 0 \end{pmatrix} \tag{94}$$

$$\begin{pmatrix} m_{00} & m_{10} & m_{01} & m_{11} \\ m_{10} & m_{20} & m_{11} & m_{21} \\ m_{01} & m_{11} & m_{02} & m_{12} \\ m_{11} & m_{21} & m_{12} & m_{22} \end{pmatrix} \begin{pmatrix} b_1^{(1,1)} \\ b_2^{(1,1)} \\ b_3^{(1,1)} \\ b_4^{(1,1)} \end{pmatrix} = \begin{pmatrix} 0 \\ 0 \\ 0 \\ 1 \end{pmatrix} \tag{95}$$

The constructed scaling function kernel and wavelets are shown in Fig. 6. The window function used is a cubic spline. The components of the dilation vector are $\varrho_1 = 1 \cdot h_{x1}, \quad \varrho_2 = 1 \cdot h_{x2}$.

4.2 Convergence rate of interpolation error

To this end, we are in a position to examine the convergence rate of this newly formed interpolants.
Recall

$$\mathscr{K}_{\varrho}^{[s]}(\cdot,\cdot) = \sum_{|\beta|=0}^{m} C_\beta \mathscr{K}_{\varrho}^{[\beta]}(\cdot,\cdot) \ . \tag{96}$$

Define the synchronized reproducing kernel interpolation formula as

$$\tilde{\mathscr{R}}_{\varrho}^{m} u(\mathbf{x}) := \int_{\Omega} \mathscr{K}_{\varrho}^{[s]}(\mathbf{y}-\mathbf{x},\mathbf{x}) u(\mathbf{y}) \mathrm{d}\Omega_y \tag{97}$$

and the moments of synchronized reproducing kernel interpolants are

$$\tilde{M}_\alpha(\mathbf{x}) := \int_{\Omega} \left(\frac{\mathbf{y}-\mathbf{x}}{\varrho}\right)^{\alpha} \mathscr{K}_{\varrho}^{[s]}(\mathbf{y}-\mathbf{x},\mathbf{x}) \mathrm{d}\Omega_{\mathbf{\Omega}} \ . \tag{98}$$

It is clear that

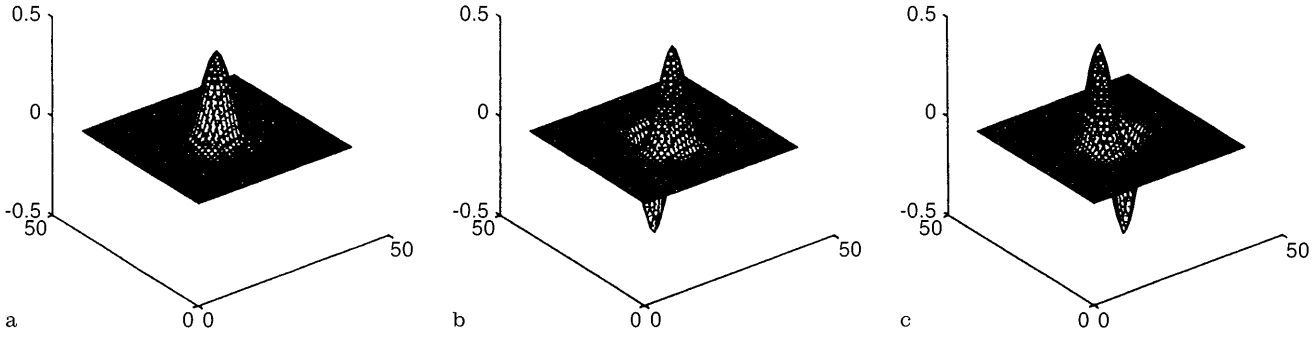

Fig. 5a–c. Scaling function kernel and wavelets for basis $(1, x_1, x_2)$: **a** Scaling function kernel; **b** The 1st wavelet; **c** The 2nd wavelet

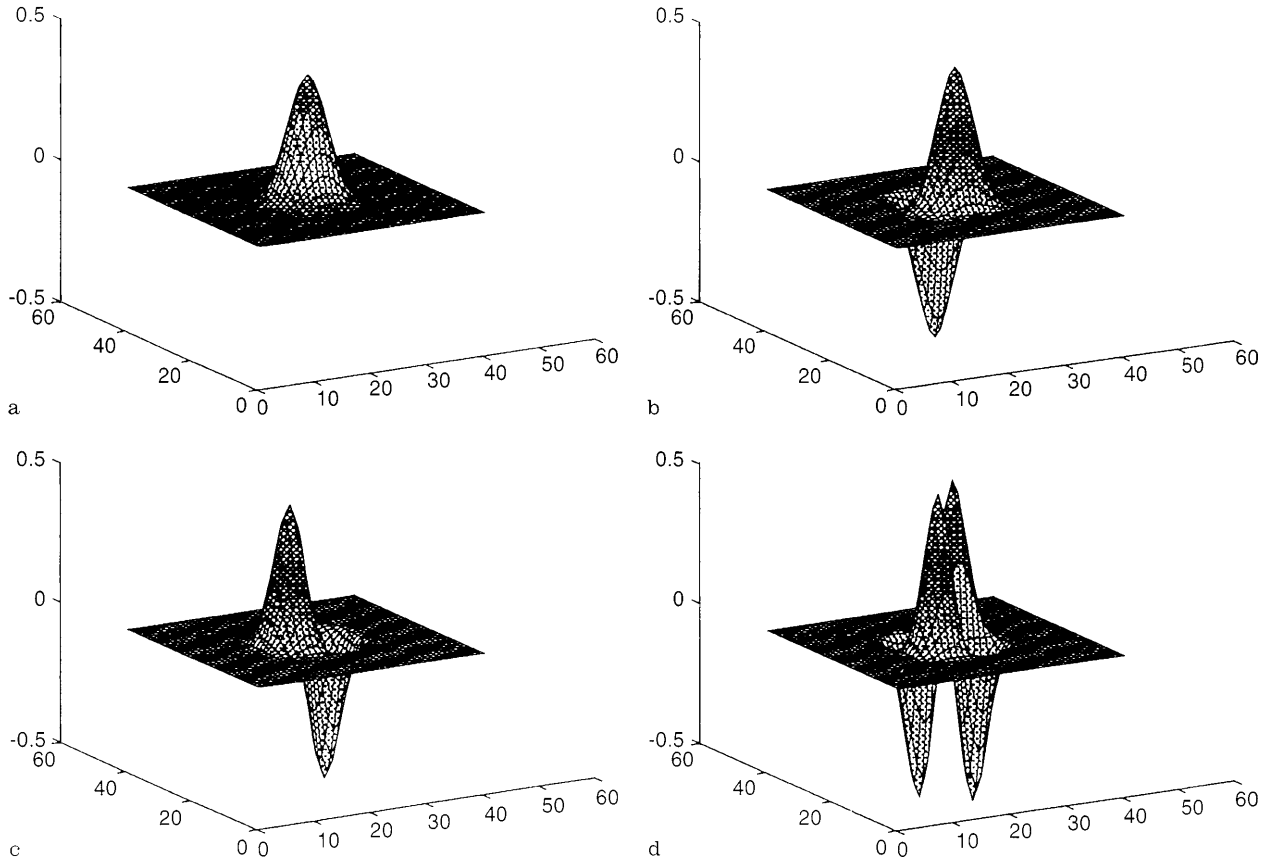

Fig. 6a–d. Scaling function kernel and wavelets for basis $(1, x_1, x_2, x_1x_2)$: **a** Scaling function kernel; **b** The 1st wavelet; **c** The 2nd wavelet; **d** The 3rd wavelet

$$\tilde{M}_\alpha(\mathbf{x}) = \sum_{|\beta|=0}^{m} C_\beta M_\alpha^{[\beta]}(\mathbf{x}) \ . \tag{99}$$

In what follows, Example (4.2) is used as a model example to demonstrate the convergence rate of the synchronized reproducing kernel.

Let the coefficient C_β in Eq. (96) be:

$$C_0 = 1, \ C_1 = C_2 = 0 \ . \tag{100}$$

In this case, the new interpolant is exactly the same as the regular reproducing kernel, i.e.

$$\mathscr{K}_\varrho^{[s]}(\cdot,\cdot) = \mathscr{K}_\varrho^{[0]}(\cdot,\cdot) \tag{101}$$

Consequently, the moments of the new reproducing kernel interpolant are unchanged, i.e.

$$\tilde{M}_0 = 1, \ \tilde{M}_1 = \tilde{M}_2 = 0, \ \tilde{M}_3(x) \neq 0 \ , \tag{102}$$

subsequently,

$$\tilde{M}_0^{(1)} = 0, \ \tilde{M}_1^{(1)} = 1!, \ \tilde{M}_2^{(1)} = 0;$$
$$\tilde{M}_0^{(2)} = 0, \ \tilde{M}_1^{(2)} = 0, \ \tilde{M}_2^{(2)} = 2! \ . \tag{103}$$

Obviously, there is no synchronized convergence effect, and the corresponding local truncation errors are shown in Table 3. From there, one can deduce that the convergence rate of the global interpolation error is still optimal, i.e. L_2 norm is in $\mathscr{O}(\varrho^3)$, H_1 norm is in $\mathscr{O}(\varrho^2)$, and H_2 norm is in $\mathscr{O}(\varrho)$.

In the second case, we choose the coefficient C_β in Eq. (96) as

$$C_0 = 1, \ C_1 = 0, \ C_2 = 1 \ . \tag{104}$$

Table 3. Optimal convergence rates

Moment conditions		$\tilde{M}_0 = 1$	$\tilde{M}_1 = 0$	$\tilde{M}_2 = 0$	$\tilde{M}_3 = \tilde{M}_3(x)$
L_2	$u - \tilde{\mathscr{R}}_\varrho^m u =$	$u(1-\tilde{M}_0)$	$-\varrho u^{(1)}\tilde{M}_1$	$-\frac{\varrho^2}{2!}u^{(2)}\tilde{M}_2$	$-\frac{\varrho^3}{3!}u^{(3)}\tilde{M}_3$
			$\mathscr{O}(\varrho)$	$\mathscr{O}(\varrho^2)$	$\mathscr{O}(\varrho^3)$
H_1	$D_x(u - \tilde{\mathscr{R}}_\varrho^m u) =$	$-\frac{1}{\varrho}u\tilde{M}_0^{(1)}$	$u^{(1)}(1-\tilde{M}_1^{(1)})$	$-\frac{\varrho}{2!}u^{(2)}\tilde{M}_2^{(1)}$	$-\frac{\varrho^2}{3!}u^{(3)}\tilde{M}_3^{(1)}$
				$\mathscr{O}(\varrho)$	$\mathscr{O}(\varrho^2)$
H_2	$D_x^2(u - \tilde{\mathscr{R}}_\varrho^m u) =$	$-\frac{1}{\varrho^2}u\tilde{M}_0^{(2)}$	$-\frac{1}{\varrho}u^{(1)}\tilde{M}_1^{(2)}$	$u^{(2)}(1-\frac{1}{2!}\tilde{M}_2^{(2)})$	$-\frac{\varrho}{3!}u^{(3)}\tilde{M}_3^{(2)}$
				$\mathscr{O}(\varrho^0)$	$\mathscr{O}(\varrho)$

Subsequently, we have

$$\tilde{M}_0 = 1,\ \tilde{M}_1 = 0,\ \text{and}\ \tilde{M}_2 = 1\ , \tag{105}$$

and

$$\begin{aligned} &\tilde{M}_0^{(1)} = 0,\ \tilde{M}_1^{(1)} = 1!,\ \tilde{M}_2^{(1)} = 0; \\ &\tilde{M}_0^{(2)} = 0,\ \tilde{M}_1^{(2)} = 0,\ \tilde{M}_2^{(2)} = 2!\ . \end{aligned} \tag{106}$$

Since $\tilde{M}_2$ is no longer zero, it pushes down the truncation error for the term, $(u - \tilde{\mathscr{R}}_\varrho^m u)$, consequently, the L_2 error norm is one order lower than that of the optimal rate, i.e. $\mathscr{O}(\varrho^2)$. Therefore, the convergence rate with respect to L_2 norm and H_1 norm are "synchronized", as indicated in Table 4, while as the convergence rate in H_2 norm remains unchanged.

This synchronized behavior becomes even more obvious in the third case, if we choose,

$$C_0 = 0, \quad C_1 = 1, \quad C_2 = 0\ . \tag{107}$$

Consequently,

$$\tilde{M}_0 = 1, \quad \tilde{M}_1 = 1, \quad \text{and} \quad \tilde{M}_2 = 0\ , \tag{108}$$

and

$$\begin{aligned} &\tilde{M}_0^{(1)} = 0, \quad \tilde{M}_1^{(1)} = 1, \quad \tilde{M}_2^{(1)} = 2; \\ &\tilde{M}_0^{(2)} = 0, \quad \tilde{M}_1^{(2)} = 0, \quad \tilde{M}_2^{(2)} = 2!\ . \end{aligned} \tag{109}$$

Because $\tilde{M}_1 \neq 0$ and $\tilde{M}_2^{(1)} \neq 0$, they further push down the order of truncation errors for both $(u - \tilde{\mathscr{R}}_\varrho^m u)$ and $D_x(u - \tilde{\mathscr{R}}_\varrho^m u)$. Accordingly, the convergence rates for both L_2 norm and H_1 norm retrieve one order lower than the optimal convergence rate, as indicated in Table 5. Thus, this particular wavelet expansion results in an synchronized interpolating scheme, in which the convergence rates of L_2 norm, H_1 norm, and H_2 norm are in the same order, i.e. $\mathscr{O}(\varrho)$.

In general, for an m-th order generating polynomial, we can choose an integer n, $0 \leq n \leq m$, and let $C_n \neq 0$, such that the convergence rate of the interpolation error of H_k norms, $0 \leq k \leq m + 1 - n$, can be synchronized at order n, i.e. $\mathscr{O}(\varrho^n)$, as stated in the following theorem.

Theorem 4.1 *Assume $u \in H^{m+1}(\Omega)$, $\phi \in H^s(\Omega)$, where $s > m + 1$. For the m-th order synchronized kernel interpolant, by fixing n, $0 \leq n \leq m$, and choosing $C_0 = 1$; $C_\beta \neq 0$, $|\beta| = n$, the following interpolation error estimate holds,*

$$\begin{aligned} &\|u - \tilde{\mathscr{R}}_\varrho^m u\|_{H^k(\Omega)} \leq C_k \varrho^n\ \|u\|_{H^{m+1}(\Omega)} \\ &0 \leq k \leq m + 1 - n \end{aligned} \tag{110}$$

The proof of the Theorem 4.1 is omitted. A detailed mathematical analysis will be presented in a forthcoming paper (Li and Liu 1997).

To validate the Theorem 4.1, we used synchronized reproducing kernel interpolants to interpolate function $\sin x$ in a 1-D line segment [0, 1]. Three polynomial bases are used ($m = 1, 2, 3$). The numerical results are displayed in Fig. 7. In Fig. 7, based on Eq. (110), we fix the index of synchronized convergence rate n. Then, for different approximation order m, one can calculate the range of affected error norm H^k, $0 \leq k \leq m + 1 - n$. For $m = 1, 2, 3$, Fig. 7 presents a complete set of results. As can be seen, the reproducing kernel interpolant has synchronized effect. For $m = 1$, the cubic spline is used as the window function; for $m = 2, 3$, the fifth order spline is used as the window function. The dilation parameters are chosen as $\varrho = ah$, where $a = 1.0$ for $m = 1$ and $a = 1.2$ for $m = 2, 3$. One may note that there is a distinction between the synchronized convergence phenomenon discussed in Sect. 3 and the synchronized reproducing kernel interpolants presented in this section. Unlike the synchronized convergence phenomenon demonstrated in Sect. 3, where the higher order H-norm convergence rates go up, the convergence rates of higher order H-norm remain the same, whereas the convergence rates of lower order error norms go down to match that of the higher order

Table 4. Synchronized convergence rates ($C_2 \neq 0$)

Moment conditions		$\tilde{M}_0 = 1$	$\tilde{M}_1 = 0$	$\tilde{M}_2 = 1$	$\tilde{M}_3 = \tilde{M}_3(x)$
L_2	$u - \tilde{\mathscr{R}}_\varrho^m u =$	$u(1 - \tilde{M}_0)$	$-\varrho u^{(1)} \tilde{M}_1$	$-\frac{\varrho^2}{2!} u^{(2)} \tilde{M}_2$	$-\frac{\varrho^3}{3!} u^{(3)} \tilde{M}_3$
			$\mathscr{O}(\varrho)$	$\mathscr{O}(\varrho^2)$	$\mathscr{O}(\varrho^3)$
H_1	$D_x(u - \tilde{\mathscr{R}}_\varrho^m u) =$	$-\frac{1}{\varrho} u \tilde{M}_0^{(1)}$	$u^{(1)}(1 - \tilde{M}_1^{(1)})$	$-\frac{\varrho}{2!} u^{(2)} \tilde{M}_2^{(1)}$	$-\frac{\varrho^2}{3!} u^{(3)} \tilde{M}_3^{(1)}$
				$\mathscr{O}(\varrho)$	$\mathscr{O}(\varrho^2)$
H_2	$D_x^2(u - \tilde{\mathscr{R}}_\varrho^m u) =$	$-\frac{1}{\varrho^2} u \tilde{M}_0^{(2)}$	$-\frac{1}{\varrho} u^{(1)} \tilde{M}_1^{(2)}$	$u^{(2)}(1 - \frac{1}{2!} \tilde{M}_2^{(2)})$	$-\frac{\varrho}{3!} u^{(3)} \tilde{M}_3^{(2)}$
				$\mathscr{O}(\varrho^0)$	$\mathscr{O}(\varrho)$

Table 5. Synchronized convergence rates ($C_1 \neq 0$)

Moment conditions		$\tilde{M}_0 = 1$	$\tilde{M}_1 = 1$	$\tilde{M}_2 = 0$	$\tilde{M}_3 = \tilde{M}_3(x)$
L_2	$u - \tilde{\mathscr{R}}_\varrho^m u =$	$u(1 - \tilde{M}_0)$	$-\varrho u^{(1)} \tilde{M}_1$	$-\frac{\varrho^2}{2!} u^{(2)} \tilde{M}_2$	$-\frac{\varrho^3}{3!} u^{(3)} \tilde{M}_3$
			$\mathscr{O}(\varrho)$	$\mathscr{O}(\varrho^2)$	$\mathscr{O}(\varrho^3)$
H_1	$D_x(u - \tilde{\mathscr{R}}_\varrho^m u) =$	$-\frac{1}{\varrho} u \tilde{M}_0^{(1)}$	$u^{(1)}(1 - \tilde{M}_1^{(1)})$	$-\frac{\varrho}{2!} u^{(2)} \tilde{M}_2^{(1)}$	$-\frac{\varrho^2}{3!} u^{(3)} \tilde{M}_3^{(1)}$
				$\mathscr{O}(\varrho)$	$\mathscr{O}(\varrho)^2$
H_2	$D_x^2(u - \tilde{\mathscr{R}}_\varrho^m u) =$	$-\frac{1}{\varrho^2} u \tilde{M}_0^{(2)}$	$-\frac{1}{\varrho} u^{(1)} \tilde{M}_1^{(2)}$	$u^{(2)}(1 - \frac{1}{2!} \tilde{M}_2^{(2)})$	$-\frac{\varrho}{3!} u^{(3)} \tilde{M}_3^{(2)}$
				$\mathscr{O}(\varrho^0)$	$\mathscr{O}(\varrho)$

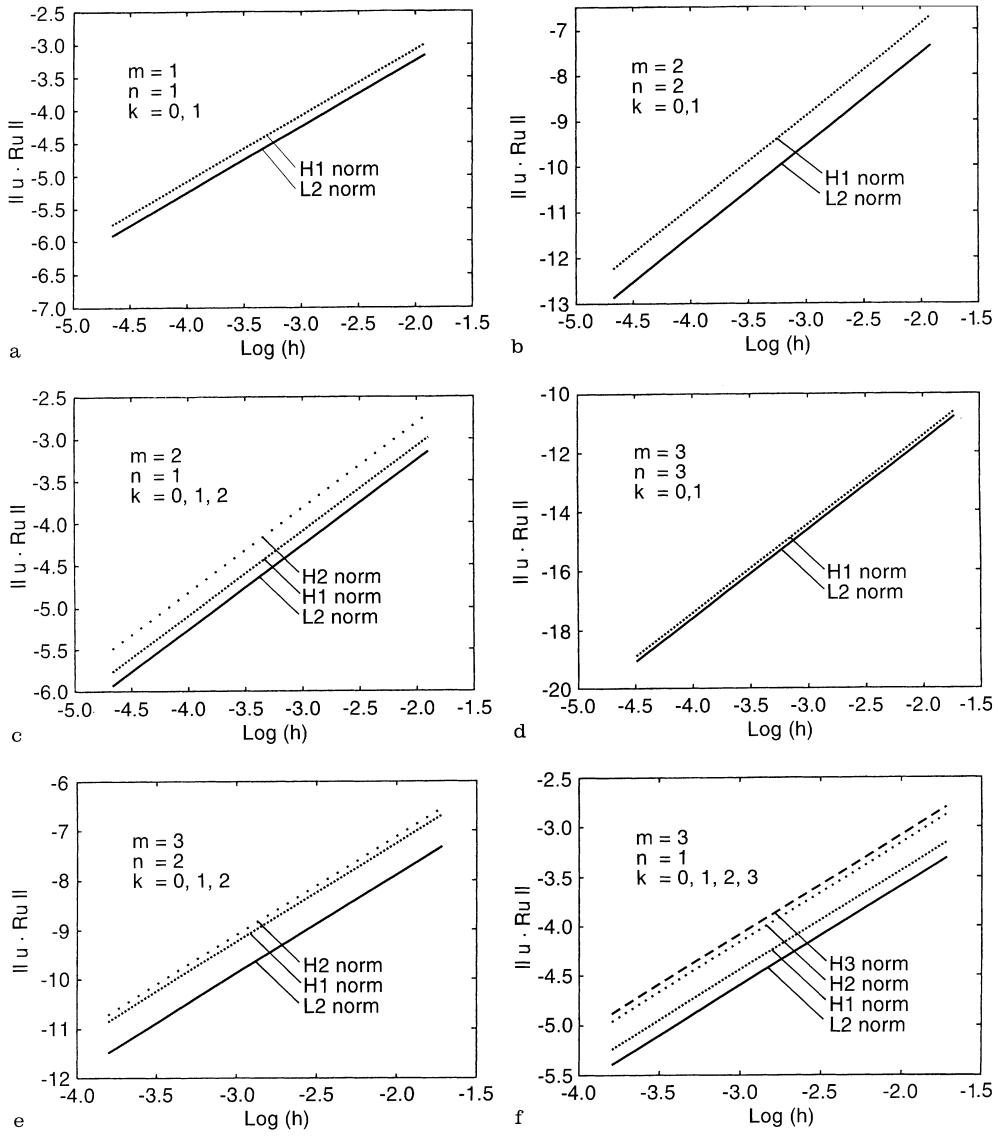

Fig. 7a–f. Convergence rates of interpolation errors for SRK interpolants; **a** Basis $(1, x)$; **b–c** Basis $(1, x, x^2)$; **d–f** Basis $(1, x, x^2, x^3)$

H-norms. Also, in Sect. 3, the particle distributions have to be uniform, whereas the synchronized reproducing kernel interpolant discussed here is still a meshless interpolant.

4.3
Application to the finite element method

The synchronized convergence phenomenon may exist in other interpolation schemes, such as Galerkin wavelet method, other meshless methods, and the finite element method as well. Certainly, it will be interesting to examine these counterparts in different interpolation frameworks. In the following examples, we shall apply the synchronized convergence concept and construction procedure to finite element method and observe the consequence.

Assume that in each element every single node is attached with an equal weight ΔV_I, and the total weight is either the length, area, or volume of the element, i.e. $\sum_{I=1}^{n} \Delta V_I = \Omega_0$. We define the finite element shape functions as

$$N^{[\beta]}(\mathbf{x}) := \mathscr{K}_{\varrho}^{[\beta]}(\mathbf{x}_I - \mathbf{x}, \mathbf{x})\Delta V_I \tag{111}$$

$$N_I^{[s]}(\mathbf{x}) := \mathscr{K}_{\varrho}^{[s]}(\mathbf{x}_I - \mathbf{x}, \mathbf{x})\Delta V_I \ . \tag{112}$$

Accordingly,

$$N_I^{[s]}(\mathbf{x}) := \sum_{|\beta|=0}^{m} C_\beta N_I^{[\beta]}(\mathbf{x}) \ . \tag{113}$$

Example 4.6 *Consider an 1-D linear master element. The master element is defined in the segment $\xi \in [-1, 1]$. There are two nodes in the element, residing at $\xi_1 = -1$ and $\xi_2 = 1$ respectively. Based on the procedure of constructing synchronized shape function, the following set of discrete moment conditions are enforced*:

$$M_0^{[0]h} = 1, \quad M_1^{[0]h} = 0, \quad |\beta| = 0 \ ; \tag{114}$$

$$M_0^{[1]h} = 0, \quad M_1^{[1]h} = 1, \quad |\beta| = 1 \ , \tag{115}$$

which yield the following equations

$$\begin{pmatrix} 1 & 1 \\ -1-\xi & 1-\xi \end{pmatrix} \begin{pmatrix} N_1^{[0]}(\xi) \\ N_2^{[0]}(\xi) \end{pmatrix} = \begin{pmatrix} 1 \\ 0 \end{pmatrix} \ , \tag{116}$$

and

$$\begin{pmatrix} 1 & 1 \\ -1-\xi & 1-\xi \end{pmatrix} \begin{pmatrix} N_1^{[1]}(\xi) \\ N_2^{[1]}(\xi) \end{pmatrix} = \begin{pmatrix} 0 \\ 1 \end{pmatrix} \ , \tag{117}$$

The solutions of (116) and (117) are the familiar linear isoparametric element shape functions, and their 1st order derivatives:

$$\begin{pmatrix} N_1^{[0]}(\xi) \\ N_2^{[0]}(\xi) \end{pmatrix} = \begin{pmatrix} \frac{1}{2}(1-\xi) \\ \frac{1}{2}(1+\xi) \end{pmatrix} \tag{118}$$

$$\begin{pmatrix} N_1^{[1]}(\xi) \\ N_2^{[1]}(\xi) \end{pmatrix} = \begin{pmatrix} -1/2 \\ 1/2 \end{pmatrix} \tag{119}$$

From (119), one can see that we recover the linear isoparametric finite element, and its synchronized part is just the 1st order derivatives. Obviously, the synchronized reproducing kernel is a natural generalization of the isoparametric finite element. The solution (119) also has an interesting interpretation. Let us look at the node at $\xi = 1$ in an extended domain $-1 \le \xi \le 3$. The synchronized part $N_2^{[1]}(\xi)$ will be

$$N_2^{[1]}(\xi) = \begin{cases} 1/2 & \forall \xi \in [-1, 1) \\ -1/2 & \forall \xi \in [1, 3] \end{cases} \tag{120}$$

Denote

$$\psi_{a,b}(x) := \frac{1}{\sqrt{a}} \psi\left(\frac{x-b}{a}\right) \ . \tag{121}$$

Then, $N_2^{[1]}(\xi)$ is simply the Haar wavelet $\psi_{4,1}(\xi)$, where

$$\psi(x) := \begin{cases} 1 & \forall x \in [0, 1/2) \\ -1 & \forall x \in [1/2, 1) \end{cases} \ . \tag{122}$$

In Fig. 8, we plot both $N_2^{[1]}(x)$ and the Haar wavelet for comparison.

Example 4.7 *Again, take the line segment* $[-1, 1]$ *as the master element. Choose* $\xi_1 = -1, \quad \xi_2 = 0$, *and* $\xi_3 = 1$. *By enforcing the m-order vanishing moment conditions for scaling function kernel* $(m = 2)$, *i.e.*

$$M_0^{[0]h} = 1, \ M_1^{[0]h} = 0, \quad \text{and}, \quad M_2^{[0]h} = 0 \ . \tag{123}$$

We have the following equation

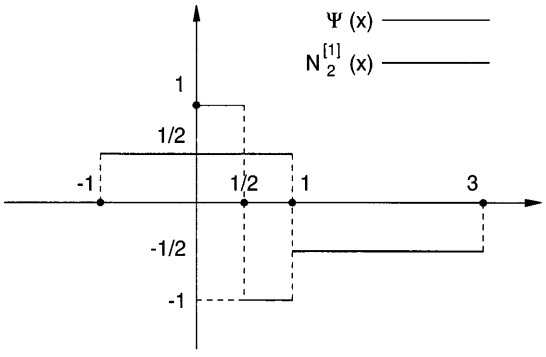

Fig. 8. Comparison between Haar wavelet and the derivative of FEM shape function

$$\begin{pmatrix} 1 & 1 & 1 \\ -1-\xi & -\xi & 1-\xi \\ (1+\xi)^2 & \xi^2 & (1-\xi)^2 \end{pmatrix} \begin{pmatrix} N_1(\xi) \\ N_2(\xi) \\ N_3(\xi) \end{pmatrix} = \begin{pmatrix} 1 \\ 0 \\ 0 \end{pmatrix} \ . \tag{124}$$

The solution is

$$\begin{pmatrix} N_1(\xi) \\ N_2(\xi) \\ N_3(\xi) \end{pmatrix} = \begin{pmatrix} \frac{1}{2}\xi(\xi-1) \\ 1-\xi^2 \\ \frac{1}{2}\xi(\xi+1) \end{pmatrix} \ , \tag{125}$$

which is exactly the same as the standard, quadratic, isoparametric shape function.

Accordingly, two sets of "vanishing moment" conditions can be imposed as

$$M_0^{[1]h} = 0, \ M_1^{[1]h} = 1, \ M_2^{[1]h} = 0 \ ; \tag{126}$$

$$M_0^{[2]h} = 0, \ M_1^{[2]h} = 0, \ M_2^{[2]h} = 1 \ . \tag{127}$$

The following two linear algebraic equations can be obtained,

$$\begin{pmatrix} 1 & 1 & 1 \\ -1-\xi & -\xi & 1-\xi \\ (1+\xi)^2 & \xi^2 & (1-\xi)^2 \end{pmatrix} \begin{pmatrix} N_1^{[1]}(\xi) \\ N_2^{[1]}(\xi) \\ N_3^{[1]}(\xi) \end{pmatrix} = \begin{pmatrix} 0 \\ 1 \\ 0 \end{pmatrix} \ . \tag{128}$$

and

$$\begin{pmatrix} 1 & 1 & 1 \\ -1-\xi & -\xi & 1-\xi \\ (1+\xi)^2 & \xi^2 & (1-\xi)^2 \end{pmatrix} \begin{pmatrix} N_1^{[2]}(\xi) \\ N_2^{[2]}(\xi) \\ N_3^{[2]}(\xi) \end{pmatrix} = \begin{pmatrix} 0 \\ 0 \\ 1 \end{pmatrix} \ . \tag{129}$$

The solutions are

$$\begin{pmatrix} N_1^{[1]}(\xi) \\ N_2^{[1]}(\xi) \\ N_3^{[1]}(\xi) \end{pmatrix} = \begin{pmatrix} \frac{1}{2}(2\xi-1) \\ -2\xi^2 \\ \frac{1}{2}(2\xi+1) \end{pmatrix} \ , \tag{130}$$

$$\begin{pmatrix} N_1^{[2]}(\xi) \\ N_2^{[2]}(\xi) \\ N_3^{[2]}(\xi) \end{pmatrix} = \begin{pmatrix} 1/2 \\ -1 \\ 1/2 \end{pmatrix} \ . \tag{131}$$

From (117), one may verify that $N_i^{[1]}(\xi)$ *are the first derivatives of* $N_i^{[0]}(\xi)$, *and* $N_i^{[2]}(\xi)$ *are proportional to the second derivatives of* $N_i^{[0]}(\xi)$.

Example 4.8 *This example is a 2-D linear four-nodes quadrilateral element. Take* ξ, η *as the local coordinate for the master element. The four nodes have the local coordinates*

$$(\xi_1, \eta_1) = (-1, -1), \ (\xi_2, \eta_2) = (1, -1),$$
$$(\xi_3, \eta_3) = (1, 1), \ (\xi_4, \eta_4) = (-1, 1) \ . \tag{132}$$

Imposing the four moment conditions for the four sets of kernel functions yield

$$\begin{pmatrix} 1 & 1 & 1 & 1 \\ -1-\xi & 1-\xi & 1-\xi & -1-\xi \\ -1-\eta & -1-\eta & 1-\eta & 1-\eta \\ (1+\xi)(1+\eta) & -(1-\xi)(1+\eta) & (1-\xi)(1-\eta) & -(1+\xi)(1-\eta) \end{pmatrix} \begin{pmatrix} N_1^{[(0,0)]} \\ N_2^{[(0,0)]} \\ N_3^{[(0,0)]} \\ N_4^{[(0,0)]} \end{pmatrix} = \begin{pmatrix} 1 \\ 0 \\ 0 \\ 0 \end{pmatrix} \tag{133}$$

$$\begin{pmatrix} 1 & 1 & 1 & 1 \\ -1-\xi & 1-\xi & 1-\xi & -1-\xi \\ -1-\eta & -1-\eta & 1-\eta & 1-\eta \\ (1+\xi)(1+\eta) & -(1-\xi)(1+\eta) & (1-\xi)(1-\eta) & -(1+\xi)(1-\eta) \end{pmatrix} \begin{pmatrix} N_1^{[(1,0)]} \\ N_2^{[(1,0)]} \\ N_3^{[(1,0)]} \\ N_4^{[(1,0)]} \end{pmatrix} = \begin{pmatrix} 0 \\ 1 \\ 0 \\ 0 \end{pmatrix} \tag{134}$$

$$\begin{pmatrix} 1 & 1 & 1 & 1 \\ -1-\xi & 1-\xi & 1-\xi & -1-\xi \\ -1-\eta & -1-\eta & 1-\eta & 1-\eta \\ (1+\xi)(1+\eta) & -(1-\xi)(1+\eta) & (1-\xi)(1-\eta) & -(1+\xi)(1-\eta) \end{pmatrix} \begin{pmatrix} N_1^{[(0,1)]} \\ N_2^{[(0,1)]} \\ N_3^{[(0,1)]} \\ N_4^{[(0,1)]} \end{pmatrix} = \begin{pmatrix} 0 \\ 0 \\ 1 \\ 0 \end{pmatrix} \tag{135}$$

$$\begin{pmatrix} 1 & 1 & 1 & 1 \\ -1-\xi & 1-\xi & 1-\xi & -1-\xi \\ -1-\eta & -1-\eta & 1-\eta & 1-\eta \\ (1+\xi)(1+\eta) & -(1-\xi)(1+\eta) & (1-\xi)(1-\eta) & -(1+\xi)(1-\eta) \end{pmatrix} \begin{pmatrix} N_1^{[(1,1)]} \\ N_2^{[(1,1)]} \\ N_3^{[(1,1)]} \\ N_4^{[(1,1)]} \end{pmatrix} = \begin{pmatrix} 0 \\ 0 \\ 0 \\ 1 \end{pmatrix} \tag{136}$$

The solutions are

$$\begin{pmatrix} N_1^{[(0,0)]}(\xi,\eta) \\ N_2^{[(0,0)]}(\xi,\eta) \\ N_3^{[(0,0)]}(\xi,\eta) \\ N_4^{[(0,0)]}(\xi,\eta) \end{pmatrix} = \begin{pmatrix} \frac{1}{4}(1-\xi)(1-\eta) \\ \frac{1}{4}(1+\xi)(1-\eta) \\ \frac{1}{4}(1+\xi)(1+\eta) \\ \frac{1}{4}(1-\xi)(1+\eta) \end{pmatrix} \; ; \tag{137}$$

$$\begin{pmatrix} N_1^{[(1,0)]}(\xi,\eta) \\ N_2^{[(1,0)]}(\xi,\eta) \\ N_3^{[(1,0)]}(\xi,\eta) \\ N_4^{[(1,0)]}(\xi,\eta) \end{pmatrix} = \begin{pmatrix} -\frac{1}{4}(1-\eta) \\ \frac{1}{4}(1-\eta) \\ \frac{1}{4}(1+\eta) \\ -\frac{1}{4}(1+\eta) \end{pmatrix} \; ; \tag{138}$$

$$\begin{pmatrix} N_1^{[(0,1)]}(\xi,\eta) \\ N_2^{[(0,1)]}(\xi,\eta) \\ N_3^{[(0,1)]}(\xi,\eta) \\ N_4^{[(0,1)]}(\xi,\eta) \end{pmatrix} = \begin{pmatrix} -\frac{1}{4}(1-\xi) \\ -\frac{1}{4}(1+\xi) \\ \frac{1}{4}(1+\xi) \\ \frac{1}{4}(1-\xi) \end{pmatrix} \; ; \tag{139}$$

$$\begin{pmatrix} N_1^{[(1,1)]}(\xi,\eta) \\ N_2^{[(1,1)]}(\xi,\eta) \\ N_3^{[(1,1)]}(\xi,\eta) \\ N_4^{[(1,1)]}(\xi,\eta) \end{pmatrix} = \begin{pmatrix} \frac{1}{4} \\ -\frac{1}{4} \\ \frac{1}{4} \\ -\frac{1}{4} \end{pmatrix} \; . \tag{140}$$

Once again, $\{N_I^{[(1,0)]}(\xi,\eta)\}$ and $\{N_I^{[(0,1)]}(\xi,\eta)\}$ recover the 1st order partial derivatives of the shape function $\{N_I^{[(0,0)]}(\xi,\eta)\}$, and $\{N_I^{[(1,1)]}(\xi,\eta)\}$ are exactly the same as $\partial^2 N^{[(1,1)]}/\partial\xi\partial\eta$.

5
Applications of synchronized reproducing kernel interpolants

There are immediate applications of the synchronized reproducing interpolants developed here. Here, main interests are in its application to numerical computations. We have employed them as weighting functions in a Petrov-Galerkin procedure. It appears that we have found a class of new shape functions that can provide excellent stabilized effect in the computations of hyperbolic partial differential equations.

5.1
Advection-diffusion equation

We first start with the one-dimensional advection-diffusion problem, which is, sometimes, called convection dominated problem. We consider the following model problem,

$$-\kappa\varphi_{,xx} + u\varphi_{,x} = f, \quad x \in (0,L) \subset \mathbb{R} \tag{141}$$

$$\varphi(0) = \varphi_0, \quad \varphi(L) = \varphi_L \; ; \tag{142}$$

where $\varphi_{,x} := \frac{d\varphi}{dx}$, $\varphi_{,xx} := \frac{d^2\varphi}{dx^2}$, and the source function $f \in \mathbb{R}$ is given. In Eq. (141), κ is the diffusive coefficient, u is the advective velocity; both of them are given positive constants.

Define the weighting function and the trial function space as follows,

$$\mathscr{V} := \{w \mid w \in H^1([0,L]), w(0) = 0, w(L) = 0;\} \tag{143}$$

$$\mathscr{S} := \{\varphi \mid \varphi \in H^1([0,L]), \varphi(0) = \varphi_0, \varphi(L) = \varphi_L;\} \tag{144}$$

The synchronized reproducing kernel shape function is defined by

$$N_I^h(x) := \mathscr{K}_{\varrho}^{[0]}(x_I - x, x)\Delta x_I \; , \; \forall x_I \in (0,L) \tag{145}$$

$$\tilde{N}_I^h(x) := \mathscr{K}_{\varrho}^{[1]}(x_I - x, x)\Delta x_I \; , \; \forall x_I \in (0,L) \; , \tag{146}$$

In the one-dimensional case, one can construct a trial function basis, $\{N_I^h \mid N_I^h \in \mathscr{V}\}$, by selecting a subset of

discrete kernel functions from reproducing kernel partition of unity. In other words, one may construct a basis

$$A := \{\mathscr{K}_{\varrho}^{[0]}(x_I - x, x) \mid \mathscr{K}_{\varrho}^{[0]}(x_I, 0) = \mathscr{K}_{\varrho}^{[0]}(x_I - L, L) = 0, \quad \forall\, x_I \in (0, L)\} \tag{147}$$

where $A \subset \{\mathscr{K}_{\varrho}^{[0]}(x_I - x, x) \mid x_I \in [0, L]\}$ and we denote the set $A_d := \{I \mid \forall \mathscr{K}_{\varrho}^{[0]}(x_I - x, x) \in A\}$ as the index set of A. Note the subtle differences between $x_I \in [0, L]$ and $x_I \in (0, L)$. Such a subset is not always available, especially, in multiple dimensional situations. Figure 9 shows an 1-D example of such trial function space, and weighting function space.

By virtue of the above argument, the following discrete trial function and weighting function can be formed,

$$\begin{aligned}\varphi^h(x) &:= \sum_{I=1}^{np} \varphi_I \mathscr{K}_{\varrho}^{[0]}(x_I - x, x)\Delta x_I \\ &= \sum_{I \in Ad} \varphi_I \mathscr{K}_{\varrho}^{[0]}(x_I - x, x)\Delta x_I \\ &\quad + \mathscr{K}_{\varrho}^{[0]}(x_0 - x, x)\Delta x_0 \varphi_0 \\ &\quad + \mathscr{K}_{\varrho}^{[0]}(x_{np} - x, x)\Delta x_{np} \varphi_L \end{aligned} \tag{148}$$

$$w^h(x) := \sum_{I \in Ad} c_I \mathscr{K}_{\varrho}^{[0]}(x_I - x, x)\Delta x_I \ , \tag{149}$$

$$\tilde{w}^h(x) := \sum_{I \in Ad} c_I \tau \mathscr{K}_{\varrho}^{[1]}(x_I - x, x)\Delta x_I \ , \tag{150}$$

where $\tau := cu/|u|$, and parameter c, a stability control parameter, is in the order $\mathcal{O}(1)$. Let $\bar{w}^h(x) := w^h(x) + \tilde{w}^h(x)$. The weighted residual form reads

$$\int_0^L \bar{w}^h(-\kappa \phi^h_{,xx} + u\varphi^h_{,x} - f)\mathrm{d}x = 0 \ . \tag{151}$$

Integration by parts yields

$$\int_0^L \left(\bar{w}^h u \varphi^h_{,x} + \bar{w}^h_{,x} \kappa \varphi^h_{,x}\right)\mathrm{d}x - \tilde{w}^h \kappa \varphi^h_{,x}|_0^L = \int_0^L \bar{w}^h f \mathrm{d}x \ , \tag{152}$$

which is an ideal Petrov-Galerkin weak form. Integration by part for the term $w^h(x)$ only, the weak form (152) can also be written as

$$\begin{aligned}&\int_0^L \left(\bar{w}^h u \varphi^h_{,x} + w^h_{,x} \kappa \varphi^h_{,x}\right)\mathrm{d}x \\ &\quad + \int_0^L \tilde{w}^h \left(-\kappa \varphi^h_{,xx} + u\varphi^h_{,x} - f\right)\mathrm{d}x = \int_0^L w^h f \,\mathrm{d}x \ .\end{aligned} \tag{153}$$

Note that $w^h(0) = w^h(L) = 0$.

The exact solution of (141)–(142) is

$$\frac{\varphi(x) - \varphi_0}{\varphi_L - \varphi_0} = \frac{1 - \exp(P_e x/L)}{1 - \exp(P_e)} \tag{154}$$

where Pe is the Peclet number that is defined as

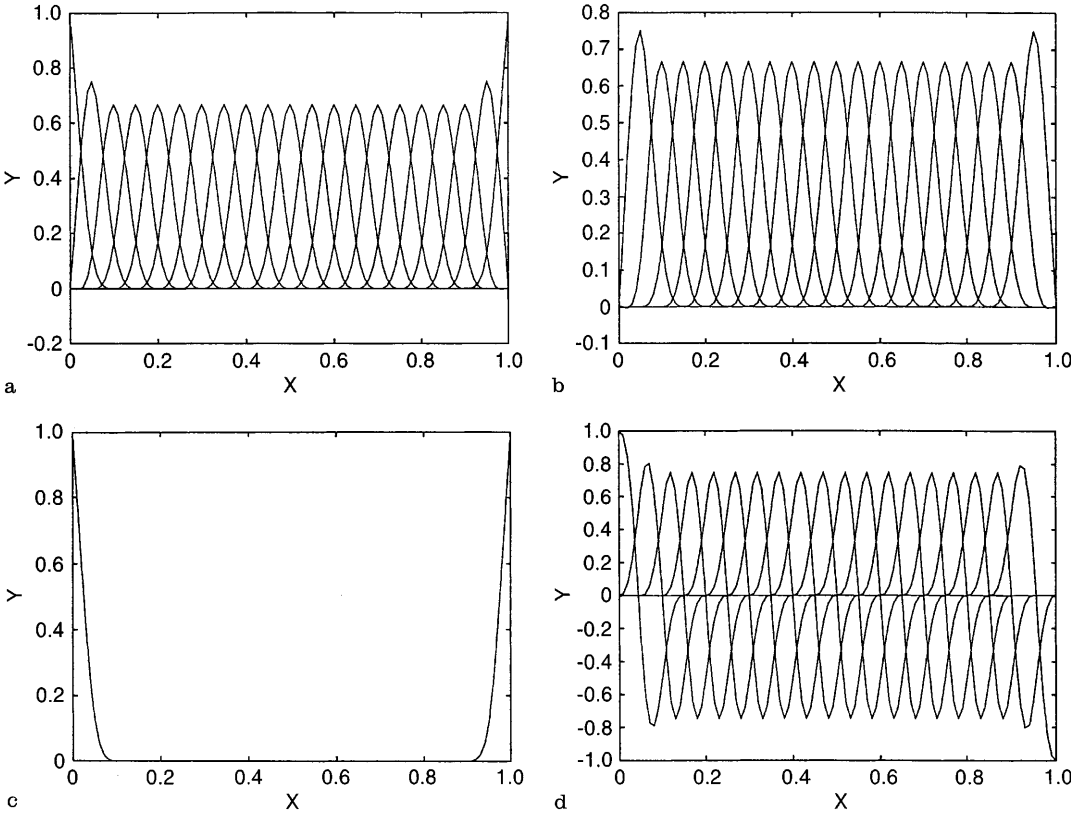

Fig. 9a–d. A decomposition of partition of unity into A and ∂A: **a** The partition of unity; **b** Basis A for w^h; **c** The set ∂A; **d** A basis for $\bar{w}^h$

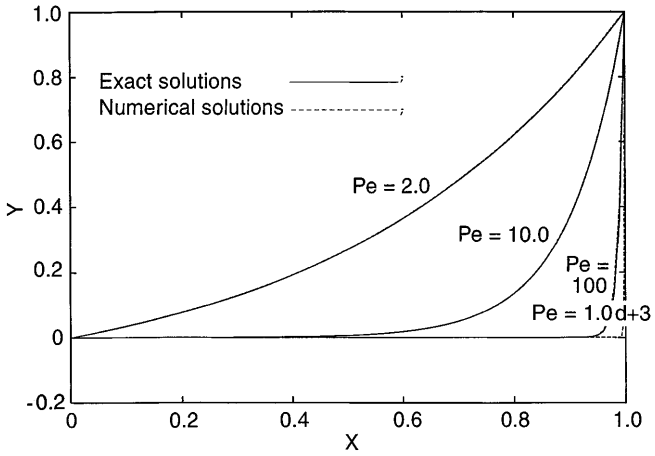

Fig. 10. The solution of one-dimensional advection diffusion

$$\mathrm{Pe} = \frac{uL}{\kappa} \quad . \tag{155}$$

Choose

$$L = 1,\ u = 1,\ \varphi_0 = 0,\ \varphi_L = 1 \quad . \tag{156}$$

Numerical computations have been performed to solve the above equations. In the actual computations, the parameter c is chosen to be 1. The synchronized shape functions used are those constructed in Example (4.1), and the dilation parameter is chosen as $\varrho = 1 \cdot h$. In Fig. (10), the exact solutions are plotted against numerical solutions obtained from the proposed Petrov-Galerkin procedure (151) at different levels of Peclet number, $\mathrm{Pe} = 2.0, 10.0, 100.0, 1000.0$. The results shown in Fig. (10) are obtained by using 101 to 201 particles. One can see that the numerical solutions are stable, and have reasonable accuracy.

5.2
Multidimensional Petrov-Galerkin formulation

For multiple dimensional problems, a formulation similar to that of the stream-line upwind/Petrov-Galerkin (SUPG) can be conveniently formed as the counterpart of the SUPG formulation proposed by Hughes and Brooks (1979, 1982).

Let $\Omega \subset \mathbb{R}^n$ be a bounded region. A model multiple dimensional advection-diffusion equation defined on Ω is described as follows,

$$\mathscr{L}\varphi^h = -\left(\kappa_{ij}\varphi^h_{,j}\right)_{,i} + u_{,i}\varphi^h_{,i} = f, \quad \forall \mathbf{x} \in \Omega \tag{157}$$

$$\varphi^h = g, \quad \forall \mathbf{x} \in \Gamma_g \tag{158}$$

$$n_i\kappa_{ij}\varphi^h_{,j} = h, \quad \forall \mathbf{x} \in \Gamma_h \quad , \tag{159}$$

where $\{\kappa_{ij}\}$ is the diffusivity tensor, and $\{u_i\}$ is the given velocity of the flow field. Let

$$\varphi^h := \sum_{I \in \bar{A}d} \varphi^h_I \mathscr{K}^{[0]}_{\varrho}(x_I - x, x)\Delta V_I \tag{160}$$

$$w^h := \sum_{I \in Ad} c_I \mathscr{K}^{[0]}_{\varrho}(x_I - x, x)\Delta V_I \tag{161}$$

where

$$\bar{A}d := \{I \mid I = 1, 2, \ldots, np\} \tag{162}$$

$$Ad := \{I \mid I \in \bar{A}d,\ \text{and}\ x_I \in \mathrm{Int}(\Omega)\} \quad . \tag{163}$$

Note that such a decomposition is not always possible. Two appropriate choices will be given later in the same section. For the moment, we assume that it could be done. For $|\beta| = 1$, we define

$$\tilde{w}^h := \hat{u}_j \tilde{w}^h_j \quad , \tag{164}$$

$$\hat{u}_j = \frac{u_j}{\|u\|}, \quad \text{and} \quad \|u\|^2 := u_i u_i \tag{165}$$

$$\tilde{w}^h_j := \sum_{I=A} c_I \mathscr{K}^{[\beta_j]}_{\varrho}(\mathbf{x}_I - \mathbf{x}, \mathbf{x})\Delta V_I \quad , \tag{166}$$

where $0 \le j \le n$ and $|\beta_j| = 1$.

Let

$$\bar{w}^h(\mathbf{x}) := w^h(\mathbf{x}) + \tau\tilde{w}^h(\mathbf{x}) \tag{167}$$

$$(f, g) := \int_\Omega fg\,\mathrm{d}\Omega \tag{168}$$

$$\mathbf{B}\left(w^h, \varphi^h\right) := \int_\Omega \left(w^h u_{,i}\varphi^h_{,i} + w^h_{,i}\kappa_{ij}\varphi^h_{,j}\right)\mathrm{d}\Omega \tag{169}$$

$$\mathbf{L}\left(w^h\right) := \int_\Omega w^h f\,\mathrm{d}\Omega + \int_{\Gamma_h} w^h h\,\mathrm{d}\Gamma_h \quad , \tag{170}$$

where parameter τ is a stability control parameter, which is in the order of $\mathscr{O}(1)$. Then, a consistent weighted residual form is

$$\left(\bar{w}^h, \mathscr{L}\varphi^h - f\right) = 0 \quad . \tag{171}$$

Integration by parts yields

$$\mathbf{B}\left(\bar{w}^h, \varphi^h\right) - \int_{\Gamma_g} \tau\tilde{w}^h n_i\kappa_{ij}\varphi^h_{,j}\,d\Gamma_g = \mathbf{L}\left(\bar{w}^h\right) \quad . \tag{172}$$

An alternative weak form can be proposed as

$$\mathbf{B}\left(w^h, \varphi^h\right) + \left(\tau\tilde{w}^h, \mathscr{L}\varphi^h\right) = \mathbf{L}\left(w^h\right) + \left(\tau\tilde{w}^h, f\right) \quad . \tag{173}$$

The benchmark problems tested are 2-D advection-diffusion problems. Let $\kappa_{ij} = \kappa\delta_{ij}$. The following particular case of Eqs. (157)–(159) is studied,

$$-\kappa\nabla^2\varphi + \mathbf{u} \cdot \nabla\varphi = f(\mathbf{x}), \quad \forall \mathbf{x} \in \Omega \tag{174}$$

$$\varphi(\mathbf{x}) = g(\mathbf{x}), \quad \forall \mathbf{x} \in \partial\Omega \quad , \tag{175}$$

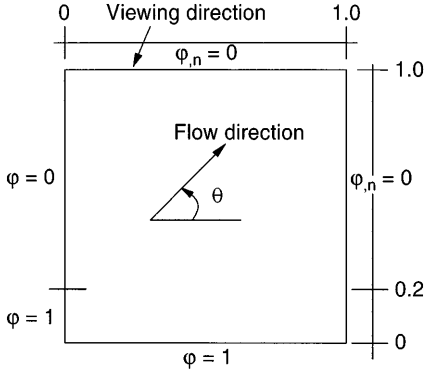

Fig. 11. Advection skew to the "mesh": Problem statement

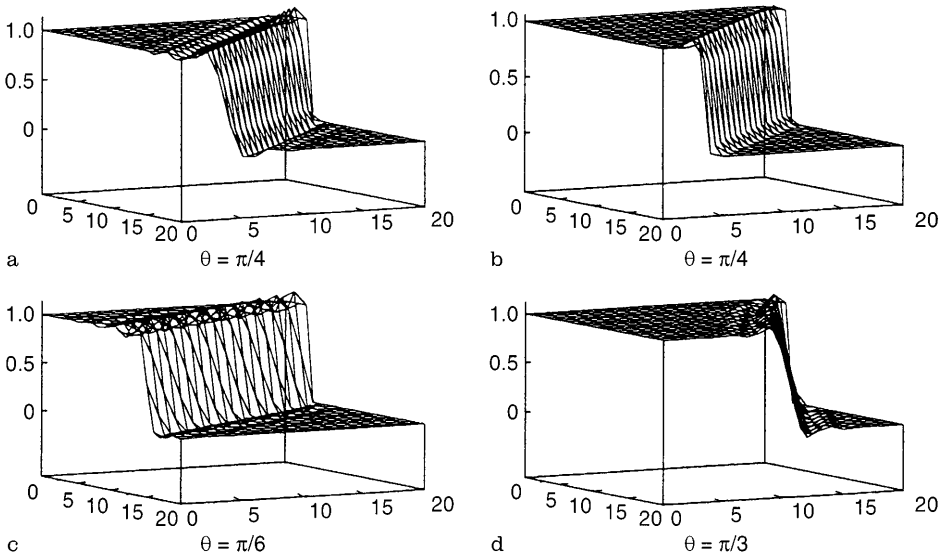

Fig. 12a–d. Numerical results for advection skew to the "mesh" **a, c, d** with full integration; **b** with reduced integration

where the diffusive coefficient, $\kappa > 0$, and **u** is the given velocity of the flow field.

The first numerical test is the so-called advection skew to the "*mesh*", which is the standard benchmark test problem in the literature (e.g. Brooks and Hughes 1992). Although there is no explicit mesh in our case, we still follow the traditional name, and put the quotation mark to make a distinction. The problem statement is described in Fig. 11. Systematic numerical computations have been done for this particular problem. A few results are selected and displayed in Fig. 12. In Fig. 12, an uniform particle distribution, 21×21, is used; no shock capturing term is involved. From the results, one can see that stable, and reasonable good numerical solutions are obtained.

The second test is the so-called cosine hill problem – advection in a rotating flow field. The problem statement is described in Fig. (13). Along the interior boundary, segment *OA*, the flow potential φ is prescribed as

$$\varphi = \frac{1}{2}[\cos(4\pi x_2 + \pi) + 1] \ . \tag{176}$$

The numerical results are shown in Fig. 14. Part a of Fig. 14 displays the profile of the function φ, and the part b of the figure shows the contour of advection-diffusion field φ. The computation is performed on a 30 by 30 particle distribution. The synchronized kernel function used is the type discussed in Example (4.4), and again, the dilation vector is chosen as $\varrho_1 = 1 \cdot h_{x1}$ and $\varrho_2 = 1 \cdot h_{x2}$. The stability control parameter τ is set at 1. In Fig. (14), one can observe that there is no phase error caused by numerical instability. In both cases, the diffusive coefficient κ is taken as 10^{-6}

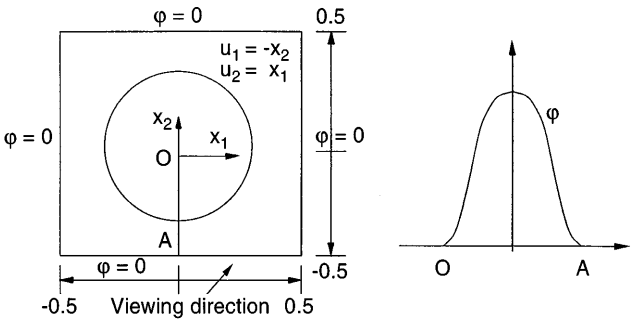

Fig. 13. Advection in a rotating flow field: Problem statement

5.3
Stokes flow problem

It is well known that the Stokes flow problem, identical to the problem of incompressible elasticity mathematically, is

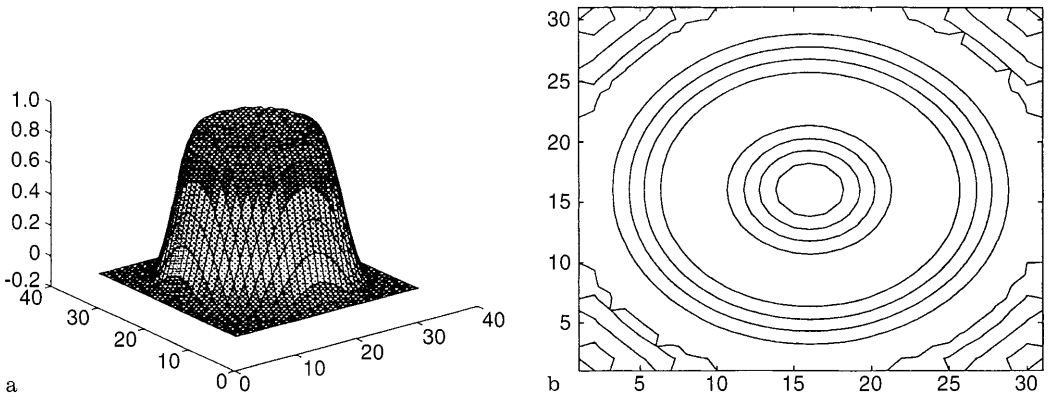

Fig. 14a, b. Numerical results for advection in a rotating field; **a** The profile of φ; **b** The contours of φ

suffering from instability in numerical simulations, if standard Bubnov-Galerkin procedure is adopted. The mathematical formulation of the problem is as follows,

$$\nabla \cdot \boldsymbol{\sigma} + \mathbf{f} = 0 \tag{177}$$

$$\nabla \cdot \mathbf{u} = 0 \tag{178}$$

where

$$\boldsymbol{\sigma} = -p\mathbf{I} + 2\mu\epsilon \tag{179}$$

$$\epsilon = \tfrac{1}{2}\left(\nabla\mathbf{u} + (\nabla\mathbf{u})^t\right) \ . \tag{180}$$

And

$$\mathbf{u}(\mathbf{x}) = \mathbf{g}(\mathbf{x}) \quad \forall \mathbf{x} \in \Gamma_g \tag{181}$$

$$(\boldsymbol{\sigma} \cdot \mathbf{n})(\mathbf{x}) = \mathbf{h}(\mathbf{x}) \quad \forall \mathbf{x} \in \Gamma_h \tag{182}$$

Many computational strategies have been invented to deal with the problem, such as penalty method, reduced integration, etc. …. It is fair to say that the best of all should be the mixed method. However, in a mixed formulation, there are certain restrictions that have to be met for displacement interpolation and pressure interpolation. The celebrated Babuška-Brezzi condition is such a requirement imposed by stability criterion. For example, it excludes the equal-order interpolations in computations. Hughes et al. (1986) proposed a Petrov-Galerkin formulation to circumvent the Babuška-Brezzi condition (CBB), such that any consistent interpolation schemes can be employed in computations. Here, following almost the exact same Petrov-Galerkin formulation, we employ the first order wavelets constructed in Example (4.5) as the additional pressure weighting functions to perform the computation, instead of using the gradient of the pressure trial function as proposed in Hughes' formulation. Let

$$\mathscr{V}^h := \{\mathbf{v} \,|\, \mathbf{v} \in H^1(\Omega), \mathbf{v}(\mathbf{x}) = 0, \ \mathbf{x} \in \Gamma_g\} \tag{183}$$

$$\mathscr{S}^h := \{\mathbf{s} \,|\, \mathbf{s} \in H^1(\Omega), \mathbf{s}(\mathbf{x}) = \mathbf{g}(\mathbf{x}), \ \mathbf{x} \in \Gamma_g\} \tag{184}$$

Assume that we can find a particle distribution that endows a partition of unity,

$$\bar{A} := \{N_I(\mathbf{x}) | N_I(\mathbf{x}) = \mathscr{K}_\varrho^{[0]}(\mathbf{x}_I - \mathbf{x}, \mathbf{x})\Delta V_1, \ 0 \le I \le np\} \ , \tag{185}$$

such that the set $\bar{A}$ can be decomposed into two independent parts,

$$\bar{A} = A \oplus \partial A \tag{186}$$

where

$$A := \{N_I(\mathbf{x}) | N_I \in \bar{A}, \ N_I(\mathbf{x}_I - \mathbf{x}, \mathbf{x}) = 0, \ \forall \mathbf{x} \in \partial\Omega\} \tag{187}$$

$$\partial A := \{N_I(\mathbf{x}) | N_I \in \bar{A}, \ \forall \mathbf{x}_I \in \partial\Omega\} \tag{188}$$

Remark 1 *The decomposition is possible if and only if,*

$$A = \{N_I | N_I \in \bar{A}, \quad X_I \in \mathrm{Int}(\Omega)\} \ . \tag{189}$$

As a matter of fact, we have used (189) *as the definition of A in* (147) *and* (163). *Not all the admissible particle distribution endow such decomposition. In those cases, extra care have to be made to deal with the essential boundary conditions. Nevertheless, in 1-D problems, this type of decompositions can be easily constructed (see Fig.* 9). In 2-*D problems, it have been found that if particular bases are used in the construction of* $\mathscr{K}_\varrho^{[0]}$, *such decomposition can also be achieved. For example, if we use the polynomial basis,* $(1, x_1, x_2, x_1x_2)$, *with the cubic spline window function, or* $(1, x_1, x_2, x_1^2, x_1x_2, x_2^2, x_1^2x_2, x_1x_2^2, x_1^2x_2^2)$, *with the fifth order spline window function, the decompositions* (186) *can be satisfied.*

We choose the following equal-order interpolation for displacements and pressure:

$$\begin{aligned}\mathbf{u}^h &:= \sum_{I\in\bar{A}} \mathbf{u}_I \mathscr{K}_\varrho^{[0]}(\mathbf{x}_I - \mathbf{x}, \mathbf{x})\Delta V_I \\ &\quad + \sum_{I\in\partial A} \tilde{\mathbf{g}}_I \mathscr{K}_\varrho^{[0]}(\mathbf{x}_I - \mathbf{x}, \mathbf{x})\Delta V_I \\ &= \mathbf{v}^h + \mathbf{g}^h \end{aligned} \tag{190}$$

$$\mathbf{w}^h := \sum_{I\in\bar{A}} \mathbf{w}_I \mathscr{K}_\varrho^{[0]}(\mathbf{x}_I - \mathbf{x}, \mathbf{x})\Delta V_I \ . \tag{191}$$

and

$$p^h := \sum_{I\in\bar{A}} p_I \mathscr{K}_\varrho^{[0]}(\mathbf{x}_I - \mathbf{x}, \mathbf{x})\Delta V_I \tag{192}$$

$$q^h := \sum_{I\in\bar{A}} q_I \mathscr{K}_\varrho^{[0]}(\mathbf{x}_I - \mathbf{x}, \mathbf{x})\Delta V_I \ . \tag{193}$$

For $\beta = 1$, let

$$\tilde{\mathbf{q}}^h := \{\tilde{q}_1^h, \tilde{q}_2^h\} \tag{194}$$

$$\tilde{q}_j^h := \frac{\varrho_j}{2\mu} \sum_{I\in\bar{A}} \tilde{q}_{Ij} \mathscr{K}_\varrho^{[\beta_j]}(\mathbf{x}_I - \mathbf{x}, \mathbf{x})\Delta V_I, \quad j = 1, 2; \tag{195}$$

where there is no summation on j, and

$$\beta_j = (1, 0), (0, 1) \ . \tag{196}$$

Then, the following CBB type of Petrov-Galerkin weak form is used in the computation,

$$\mathbf{B}_\tau(\mathbf{w}^h, q^h, \tilde{\mathbf{q}}^h, \mathbf{v}^h, p^h) = \mathbf{L}_\tau(\mathbf{w}^h, q^h, \tilde{\mathbf{q}}^h) \tag{197}$$

where

$$\begin{aligned}\mathbf{B}_\tau(\mathbf{w}^h, q^h, \tilde{\mathbf{q}}^h, \mathbf{v}^h, p^h) &:= (\epsilon(\mathbf{w}^h), 2\mu\epsilon(\mathbf{v}^h)) \\ &\quad - (\nabla \cdot \mathbf{w}^h, p^h) + (q^h, \nabla \cdot \mathbf{v}^h) \\ &\quad (\tau\tilde{\mathbf{q}}^h, \nabla p^h - 2\mu\nabla \cdot \epsilon(\mathbf{v}^h)) \end{aligned} \tag{198}$$

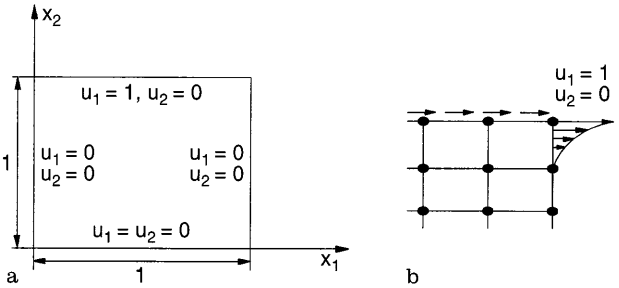

Fig. 15a, b. The cavity problem; **a** Problem statement; **b** Detail of boundary condition at the corner

and

$$\mathbf{L}_\tau(\mathbf{w}^h, q^h, \tilde{\mathbf{q}}^h) := (\mathbf{w}^h + \tau\tilde{\mathbf{q}}^h, \mathbf{f}) + (\mathbf{w}^h, h)_{\Gamma_h} - (\epsilon(\mathbf{w}^h), 2\mu\epsilon(\mathbf{g}^h)) - (q^h, \nabla\cdot\mathbf{g}^h) + (\tau\tilde{\mathbf{q}}^h, 2\mu\nabla\cdot\epsilon(\mathbf{g}^h)) \quad (199)$$

where parameter τ is the stability control parameter, which is in the order $\mathcal{O}(1)$.

In numerical experiments, the well known cavity problem is tested. It is a driven cavity flow problem with "leaky lid" boundary condition. The problem statement is shown in Fig. 15. The synchronized reproducing kernel interpolants developed in both Examples (4.4) and (4.5) are employed in the computation. Since the interpolation field is assumed to be linear, the terms that involve second derivatives are neglected, though they could be included. The results presented in Fig. 16 and Fig. 17 are based on a 11×11 particle distribution on an unit square. In all the computations, 2-D cubic spline is used as the window function, and the dilation vector is chosen as $\varrho_1 = 1 \cdot h_{x_1}, \varrho_2 = 1 \cdot h_{x_2}$. Figure 16 shows the pressure profile of the cavity problem. Part a is the numerical result obtained from Petrov-Galerkin formulation based on Eq. (197). Part b is the numerical results obtained from regular Galerkin method, from which, the pressure distribution exhibits apparent spurious pressure mode. In Fig. 17, the pressure contour and the velocity field, or the field of streamline, are displayed; both of them are obtained from the Petrov-Galerkin formulation (197).

6 Conclusion

It is a novel attempt to combine scaling function kernel, a partition of unity, and its associated wavelets to form a synchronized reproducing kernel, which can result in new options and yields positive ramifications in numerical computations. The specific construction scheme shown in this paper is under the framework of RPKM. It is possible that the same concept is applicable to other meshless methods, Galerkin-wavelet method, finite element method, partition of unity methods in general. This new development in interpolation construction may help us to design a new generation of partition of unity methods with the multiple scale computational capability.

Regarding to the applications of the synchronized reproducing kernel interpolants, as have been discussed in Sect. 5, the synchronized reproducing kernel interpolant can be effectively used as a weighting function in a Petrov-Galerkin procedure to stabilize the numerical computations. The contribution of this finding is that any complete, consistent interpolant combining with a compatible wavelet interpolant can provide a class of weighting functions for relevant Petrov-Galerkin procedures. This may be true not only for meshless methods, but also for spline interpolants, and any other Galerkin wavelet

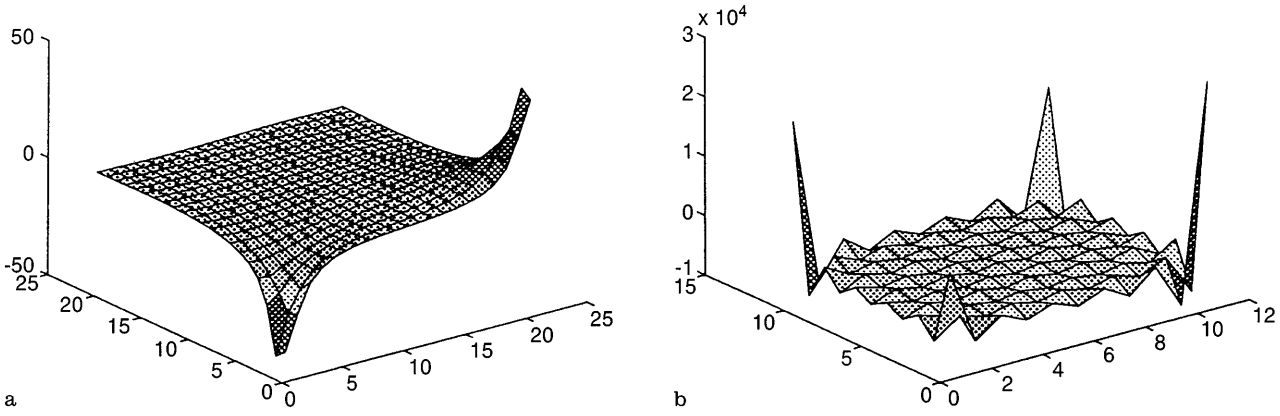

Fig. 16a, b. Pressure elevation: **a** Petrov-Galerkin solution; **b** Regular Galerkin solution

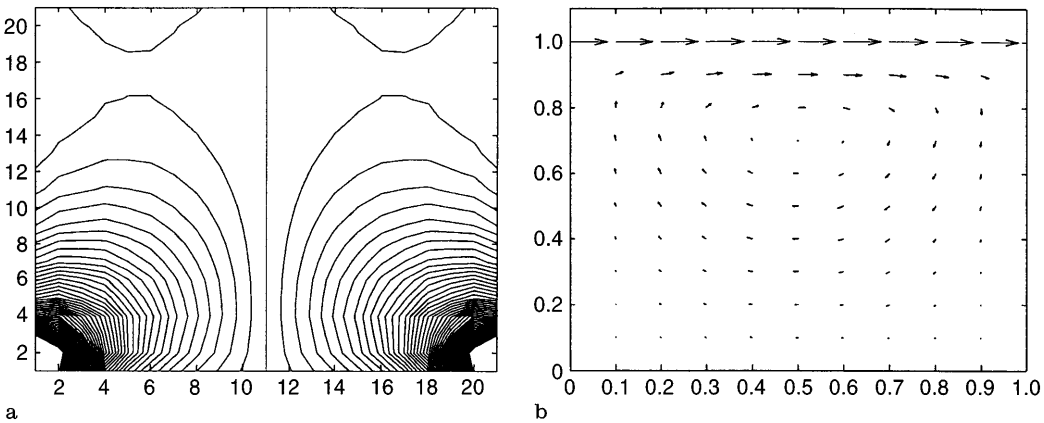

Fig. 17a, b. Numerical results of cavity problem: **a** Pressure contours; **b** Velocity field

methods. This is the generalization of the early stabilized recipe: *weighting function = original interpolant plus the 1st derivative of the interpolant*. Instead, we offer a new recipe: *weighting function = original interpolant plus the 1st wavelet*. This gives us another angle to look at stabilized methods, and deepens our understanding why the old formula works.

There are some interesting and alluring questions left in our analysis: are the wavelet functions generated here linearly independent with the scaling function kernel? If they are, will the wavelet solutions together with the scaling kernel solution form the solution in the next scale? These are the questions ultimately related with how multiple scale reproducing kernel should be formed. Moreover, one may also ask: do we find a new class of wavelets, or a new method to construct wavelets with high regularity? The significance is an obvious one. It may be too early to draw any concrete conclusion, however, it seems to us that the future is promising.

References

Adams RA (1975) Sobolev Space. Academic Press, New York

Belytschko T, Krongauz Y, Organ D, Krysl P (1996) Meshless methods: An overview and recent developments. Comput. Meth. Appl. Mech. Eng. 139: 3–48

Boor C de, Jia RO (1985) Controlled approximation and a characterization of the local approximation order. Proc. Am. Math. Soc. 95: 547–553

Brooks AN, Hughes TJR (1982) Streamline upwind/Petrov-Galerkin formulations for convection dominated flows with particular emphasis on the incompressible Navier-Stokes equations. Comput. Meth. Appl. Mech. Eng. 32: 199–259

Chui CK (1992) *An Introduction to wavelets*, Academic Press, Boston

Daubechies I (1992) Ten Lectures on Wavelets. SIAM, Philadelphia

Hughes TJR, Brooks A (1979) A multi-dimensional upwind scheme with no crosswind diffusion. In: Hughes, T.J.R. (ed) Finite Element Methods for Convection Dominated Flows, ASME, AMD 34: 19–35

Hughes TJR, Franca LP, Balestra M (1986) A new finite element formulation for computational dynamics V: Circumventing the Babuš-Brezzi condition: A stable Petrov-Galerkin formulation of the Stokes problem accommodating equal-order interpolations. Comput. Meth. Appl. Mech. Eng. 59: 85–99

Kaiser G (1994) A Friendly Guide to Wavelets. Birkhäuser, Boston, Basel, Berlin

Li S, Liu WK (1996) Moving least square reproducing kernel method (II) Fourier analysis. Comput. Meth. Appl. Mech. Eng. 139: 159–193

Li S, Liu WK (1997) Moving least square reproducing kernel method (III) Multiple wavelet expansion. Comput. Meth. Appl. Mech. Eng. (in prep.)

Liu WK (1995) Wavelet and multiple scale reproducing kernel method. USACM Bulletin 8: 3–16

Liu WK, Chen Y (1995) Wavelet and multiple scale reproducing kernel particle methods. Int. J. Num. Meth. Fluids 21: 901–933

Liu WK, Jun S, Zhang S (1995) Reproducing kernel particle methods. Int. J. Num. Meth. Fluids 20: 1081–1106

Liu WK, Chen Y, Chang CT, Belytschko T (1996) Advances in multiple scale kernel particle methods. Comput. Mech. 18: 73–111

Liu WK, Chen Y, Uras RA, Chang CT (1996) Generalized multiple scale reproducing kernel particle methods. Comput. Meth. Appl. Mech. Eng. 139: 91–158

Liu WK, Li S, Belytschko T (1997) Moving least square reproducing kernel method (I) Methodology and convergence. Comput. Meth. Appl. Mech. Eng. vol. 143, pp 113–154

Meyer Y (1993) Wavelets: algorithms & applications. SIAM, Philadelphia

Strang G, Fix G (1973) A Fourier analysis of finite element method. In: Constructive Aspects of Functional Analysis. Edizioni Cremones, Rome